
Toward Structural Multimodal Representations: Specialization, Selection, and Sparsification via Mixture-of-Experts

Hahyeon Choi¹ Nojun Kwak¹

Abstract

We propose S3 (Specialization, Selection, Sparsification), a framework that rethinks multimodal learning through a structural perspective. Instead of encoding all signals into a fixed embedding, S3 decomposes multimodal inputs into semantic experts and selectively routes them for each task. *Specialization* forms concept-level experts in a shared latent space, *Selection* adapts routing for task-specific needs, and *Sparsification* prunes low-utility paths to yield compact, information-minimal representations. Across four MultiBench benchmarks, S3 improves accuracy and shows a consistent reverse U-shaped sparsity–performance trend, with peak performance at intermediate sparsity. These results suggest that structuring multimodal representations as selectable semantic components provides a practical and principled alternative to contrastive learning or InfoMax-driven approaches.

1. Introduction

Multimodal data capture the same event through different perceptual channels, providing rich and complementary signals (Schrodi et al., 2025; Liao et al., 2025; Liang et al., 2022). However, the information from each modality is inherently asymmetric, as they differ in resolution, coverage, and noise characteristics. Moreover, the semantic overlap between modalities is context-dependent. Each paired sample, therefore, consists of a unique combination of shared and modality-unique information. While humans naturally integrate such heterogeneous signals (Ernst & Bühlhoff, 2004; Ghazanfar & Schroeder, 2006), learning algorithms must explicitly determine what to align, what to retain, and what to discard, making multimodal representation learning (MMRL) fundamentally challenging (Locatello et al., 2019;

Tishby & Zaslavsky, 2015; Yu et al., 2026).

Most existing MMRL approaches fall into two dominant paradigms. Contrastive learning methods align paired modalities by projecting them into a shared representation space (Girdhar et al., 2023; Jia et al., 2021). While effective at learning stable shared embeddings, this often comes at the cost of discarding task-relevant but modality-unique cues (Liang et al., 2023; Wang et al., 2025). The second approach, known as InfoMax-style (Linsker, 1988) methods, aim to preserve all information (Liu et al., 2023; Pan et al., 2021; Lee & Pavlovic, 2021). However, this often results in redundant representations cluttered with task-irrelevant information (Poole et al., 2020; Soatto & Chiuseo, 2016). We argue that these limitations stem not only from suboptimal objectives but also from a lack of structural inductive biases. While semantic information is heterogeneously distributed across modalities, most models collapse it into a single, uniform representation, failing to adaptively capture task-relevant information and discard irrelevant variability.

To address this, we propose a structural perspective on MMRL. Rather than refining objectives alone, we explicitly decompose multimodal inputs into interpretable semantic units. This idea draws inspiration from recent reinterpretations of Mixture-of-Experts (MoE) (Park et al., 2025; Yang et al., 2025), which treat experts not merely as tools for parameter scaling, but as semantically specialized components that enhance model interpretability and manipulability. Building on this view, we associate each expert in our model with a distinct concept, dynamically composed based on task demands. Such structured representation offers fine-grained control over what information to retain or discard. Moreover, by grounding alignment in experts consistently activated by shared concepts across data samples, the model can effectively mitigate cross-modal asymmetry while preserving modality-specific nuances.

Building on this structural view, we introduce S3 (Specialization, Selection, Sparsification), a framework that restructures MMRL into three stages. (1) Specialization decomposes multimodal signals into concept-level experts, enabling distributed alignment within a structured semantic space. This representation mitigates cross-modal asymmetry and provides a semantic basis for task-specific selection. (2) Selection subsequently navigates this fixed latent

¹Seoul National University, Seoul, South Korea. Correspondence to: Hahyeon Choi <hahyeon.choi@snu.ac.kr>, Nojun Kwak <nojunk@snu.ac.kr>.

space by adapting the routing mechanism, activating task-relevant experts to construct compact, task-focused representations. (3) Sparsification further refines the model at inference time. By pruning low-contribution routing paths, it yields Information-Minimal yet Task-Sufficient representations without additional training.

Extensive experiments show that S3 consistently outperforms prior methods and maintains structural consistency across four MultiBench (Liang et al., 2021) benchmarks. We find that its routing and sparsification behaviors follow predictable patterns shaped by semantic granularity. Notably, we observe that the sparsification process reveals a reverse U-shaped trend in performance: accuracy peaks at an optimal sparsity level that suppresses task-irrelevant noise while preserving essential signals. These findings support our central hypothesis: structuring multimodal representations as selectable semantic components enables more controllable and efficient information use. S3 thus offers a practical and theoretically grounded path toward *Task-Sufficient* and *Information-Minimal* MMRL.

2. A Fundamental Limitation of Existing Multimodal Representation Learning

We consider the self-supervised multimodal setting to analyze limitations of prior MMRL methods. For clarity, we focus on two modalities, denoted by the set $\mathcal{M} = \{1, 2\}$, although the formulation and results naturally extend to an arbitrary number of modalities. Let $X^m \sim p_{X^m}(\cdot)$ denote the input for modality $m \in \mathcal{M}$. Each encoder f^m maps the input to a stochastic latent representation $Z^m = f^m(X^m)$. Since the downstream task label Y is inaccessible during training, the learning process follows the Markov chain:

$$Y \rightarrow (X^1, X^2) \rightarrow (Z^1, Z^2). \quad (1)$$

Proposition 2.1 (Data Processing Inequality). *If (X^1, X^2) , (Z^1, Z^2) , and Y satisfy the Markov chain in Equation (1), then the Data Processing Inequality (DPI) implies:*

$$I(X^1, X^2; Y) \geq I(Z^1, Z^2; Y). \quad (2)$$

Equality holds if and only if (Z^1, Z^2) constitutes a sufficient statistic for Y (Soatto & Chiuseo, 2016).

Thus, once any Y -relevant information is lost during encoding, it cannot be recovered by downstream predictors, making Bayes-optimal performance unattainable. A detailed proof of Proposition 2.1 is provided in Section D.1.

2.1. Contrastive Learning: Modality-Aligned but Shared-Only Representations

Multimodal contrastive learning promotes cross-modal alignment by maximizing the mutual information between paired modalities (Almudévar et al., 2025; Arandjelovic & Zisserman, 2017). Let f_{CL}^m be the contrastively-learned encoder, producing a stochastic representation $Z_{\text{CL}}^m = f_{\text{CL}}^m(X^m)$, whose objective can be written as:

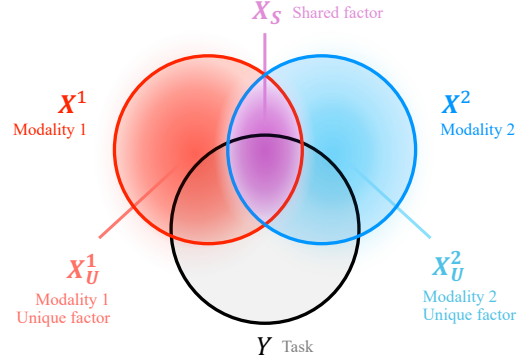


Figure 1. Latent factor decomposition of multimodal inputs into shared factor X_S and modality-unique factors (X_U^1, X_U^2). The downstream task Y may depend on some subset of them.

$$\max_{f_{\text{CL}}^1, f_{\text{CL}}^2} [I(Z_{\text{CL}}^1; X^2) + I(X^1; Z_{\text{CL}}^2)]. \quad (3)$$

While this objective encourages the encoders to capture cross-modal dependencies, it systematically suppresses task-relevant signals when the downstream task depends on modality-unique cues. To formalize this limitation, we model the latent structure of multimodal inputs using the following factorization.

Definition 2.2 (Multimodal Latent Factor Model). Each modality input X^m consists of a shared factor X_S and a modality-unique factor X_U^m :

$$X^1 = (X_S, X_U^1), \quad X^2 = (X_S, X_U^2), \quad (4)$$

and these factors satisfy the independence conditions:

$$X_S \perp X_U^1, \quad X_S \perp X_U^2, \quad X_U^1 \perp X_U^2. \quad (5)$$

This structure is illustrated in Figure 1, which depicts the decomposition into shared and modality-unique factors.

Proposition 2.3 (Mutual Information Decomposition). *Under Definition 2.2, the mutual information between modalities satisfies*

$$I(X^1; X^2) = H(X_S), \quad (6)$$

where $H(\cdot)$ denotes the entropy. In other words, the modality-unique factors X_U^1 and X_U^2 make no contribution to the mutual information between the modalities.

By Proposition 2.3, the theoretical optimum of the contrastive objective depends only on the shared factor X_S . This optimal structure offers no theoretical incentive to preserve modality-unique information X_U^m . Consequently, the contrastive representations Z_{CL}^m are effectively characterized by the following Markov chain:

$$Y \rightarrow (X_S, X_U^1, X_U^2) \rightarrow X_S \rightarrow (Z_{\text{CL}}^1, Z_{\text{CL}}^2). \quad (7)$$

We now consider the downstream setting in which the task depends on modality-unique factors.

Definition 2.4 (Task Relevance of Unique Factors). We say that the downstream task Y depends on modality-unique factors when the following condition holds:

$$I(X_U^1, X_U^2; Y) > 0. \quad (8)$$

Proposition 2.5 (Fundamental Limitation of Contrastive Representations). *If the condition in Definition 2.4 holds, then the contrastively-learned representations satisfy:*

$$I(X^1, X^2; Y) > I(Z_{CL}^1, Z_{CL}^2; Y). \quad (9)$$

This strict inequality follows directly from Proposition 2.1. It implies that Z_{CL}^m cannot serve as a sufficient statistic when the task depends on modality-unique features. Despite strong cross-modal alignment, the contrastive objective lacks an explicit mechanism to retain modality-unique features, resulting in an inevitable loss of task-relevant information. Proofs are provided in Sections D.2 and D.3.

2.2. InfoMax: Preserving Everything, Losing Focus

As discussed in Section 2.1, contrastive learning aligns shared information but overlooks modality-unique factors critical for certain tasks. To address this limitation, recent works (Wang et al., 2025; Liu et al., 2023; Pan et al., 2021) adopt InfoMax-style approaches (Linsker, 1988; Hjelm et al., 2019) that aim to preserve both shared and modality-unique information. In this setting, each input X^m is encoded into a shared representation Z_S and a modality-unique representation Z_U^m via encoders f_{\max}^m , modeled as $(Z_S, Z_U^m) = f_{\max}^m(X^m)$. These methods typically optimize

$$\max_{f_{\max}^1, f_{\max}^2} \sum_m [I(Z_S; X^m) + I(Z_U^m; X^m | Z_S)]. \quad (10)$$

Defining $Z_{\max}^m = (Z_S, Z_U^m)$, the objective becomes, by the chain rule, equivalent to maximizing $\sum_m I(Z_{\max}^m; X^m)$, which encourages the model to retain all information from the input. As a result, InfoMax is possible to satisfy the equality condition in Proposition 2.1 and aims to produce a Y -sufficient representation. However, it also inherently retains substantial task-irrelevant information.

Definition 2.6 (Task-Irrelevant Information). The task-irrelevant information captured by representation Z^m from X^m , conditioned on Y , is defined as:

$$I(Z^m; X^m | Y). \quad (11)$$

Under the Markov chain in Equation (1), the InfoMax objective decomposes as:

$$\max_{f_{\max}^1, f_{\max}^2} \sum_m [I(Z_{\max}^m; Y) + I(Z_{\max}^m; X^m | Y)]. \quad (12)$$

This decomposition reveals that InfoMax simultaneously maximizes both task-relevant ($I(Z_{\max}^m; Y)$) and task-irrelevant ($I(Z_{\max}^m; X^m | Y)$) information. Retaining such irrelevant information has been widely reported as detrimental to downstream performance (Liang et al., 2023; Soatto &

Chiuso, 2016). In particular, Poole et al. (2020) introduced the InfoMin principle in the unimodal setting, emphasizing that representations should be sufficient for the task but minimal with respect to the input. In summary, while InfoMax-based approaches alleviate the shared-only bias of contrastive learning, they remain suboptimal due to their inability to suppress task-irrelevant information.

3. Towards Structurally Optimal Multimodal Representations

3.1. Task-Sufficiency and Information-Minimality

As discussed in Section 2, existing approaches fail in complementary ways. Contrastive learning discards modality-unique signals essential for certain tasks, whereas InfoMax-style methods preserve excessive task-irrelevant information. This motivates the need to precisely characterize the balance between information retention and suppression in multimodal settings. To this end, we extend the InfoMin principle (Poole et al., 2020) to multimodal settings and formalize the conditions that an optimal task-specific representation (Z_Y^{1*}, Z_Y^{2*}) must satisfy. Under the Markov chain in Equation (1), such representations must preserve all information relevant to the target Y . This corresponds to the equality condition in Proposition 2.1.

Definition 3.1 (Task-Sufficiency). (Z_Y^{1*}, Z_Y^{2*}) satisfies Task-Sufficiency if and only if it is a sufficient statistic for Y :

$$I(Z_Y^{1*}, Z_Y^{2*}; Y) = I(X^1, X^2; Y). \quad (13)$$

However, Task-Sufficiency alone does not ensure the exclusion of irrelevant factors. To be optimal, representations must exclude all information that is independent of Y .

Definition 3.2 (Information-Minimality). (Z_Y^{1*}, Z_Y^{2*}) satisfies Information-Minimality if it is conditionally independent of the inputs (X^1, X^2) given Y :

$$I(Z_Y^{1*}, Z_Y^{2*}; X^1, X^2 | Y) = 0. \quad (14)$$

Together, these two conditions imply that (Z_Y^{1*}, Z_Y^{2*}) forms a minimal sufficient statistic for Y (Soatto & Chiuso, 2014), which we treat as our theoretical optimum.

3.2. From Monolithic to Structured Representations

While these formulations define an ideal target, achieving such optimality in practice is challenging. Multimodal inputs often consist of complex mixtures of shared and modality-unique factors, whose task-relevance varies across samples. Consequently, a single monolithic embedding cannot flexibly adapt to such variability, limiting the generalization and expressivity of learned representations.

To overcome this limitation, we shift towards a structured representation that organizes information into semantically meaningful components. We structure representations based on latent semantic concepts that may appear in one or both

modalities. Instead of aligning raw inputs directly, we aim to align distributions over concept-specific subspaces, which allows for the flexible reuse of shared semantics while accommodating modality-specific nuances. This perspective offers potential robustness to cross-modal asymmetry and supports more principled generalization. We formalize this intuition through the notion of Distributional Semantic Coherence (DSC), which forms the foundation of our proposed S3 framework.

Definition 3.3 (Latent Semantic Concept Space). Let \mathcal{Z} denote the joint latent representation space. We assume a set of latent semantic concepts \mathcal{C} and model \mathcal{Z} as a structured space composed of concept-wise subspaces $\{\mathcal{Z}_c\}_{c \in \mathcal{C}}$ such that $\mathcal{Z} = \bigoplus_{c \in \mathcal{C}} \mathcal{Z}_c$, where each $c \in \mathcal{C}$ corresponds to a distinct latent semantic concept. For an input sample x^m , a realization of X^m , the set of active concepts is defined as

$$C^m(x^m) = \{c \in \mathcal{C} \mid \|\pi_c(f^m(x^m))\| > \epsilon\}, \quad (15)$$

where $\pi_c : \mathcal{Z} \rightarrow \mathcal{Z}_c$ is the concept-wise projection operator and $\epsilon \geq 0$ is a sparsity threshold.

Definition 3.4 (Distributional Semantic Coherence). A concept $c \in \mathcal{C}$ is shareable if $\Pr(c \in C^1(X^1) \cap C^2(X^2)) > 0^1$. A multimodal representation satisfies DSC if, for every shareable concept c , the distributions of its concept-specific latent variables are identical across modalities:

$$p(\pi_c(Z^1) \mid c \in C^1(X^1)) = p(\pi_c(Z^2) \mid c \in C^2(X^2)). \quad (16)$$

4. Preliminaries

In this section, we summarize the operating principles of the Mixture-of-Experts (MoE) architecture (Figure 2) that underpins the proposed S3 framework. For notational simplicity, we omit the modality index m throughout Section 4.

4.1. Transformer

The Transformer (Vaswani et al., 2017) consists of L stacked layers, each composed of a Multi-Head Attention (MHA) module followed by a Feed-Forward Network (FFN). We focus our description on the FFN computation, as it serves as the baseline component replaced by the MoE layer. Given an intermediate token representation $\mathbf{x} \in \mathbb{R}^{D_{\text{model}}}$ at a particular encoder layer, the FFN applies two linear transformations with a nonlinear activation ϕ (e.g., GeLU or ReLU):

$$\text{FFN}(\mathbf{x}) = \mathbf{W}_2 \phi(\mathbf{W}_1 \mathbf{x} + \mathbf{b}_1) + \mathbf{b}_2, \quad (17)$$

where $\mathbf{W}_1 \in \mathbb{R}^{D_{\text{ffn}} \times D_{\text{model}}}$, $\mathbf{b}_1 \in \mathbb{R}^{D_{\text{ffn}}}$, $\mathbf{W}_2 \in \mathbb{R}^{D_{\text{model}} \times D_{\text{ffn}}}$, $\mathbf{b}_2 \in \mathbb{R}^{D_{\text{model}}}$ are the learnable parameters of the FFN. The hidden dimension typically follows $D_{\text{ffn}} = 4 \cdot D_{\text{model}}$ (Radford et al., 2018; Rae et al., 2021; Touvron et al., 2023).

¹Consider (image, audio) data. If the dataset contains a (DOG image, DOG sound) pair, the concept of DOG is shareable. However, the concept of a color (e.g., BLACK) cannot be shared because audio data cannot contain the color concept.

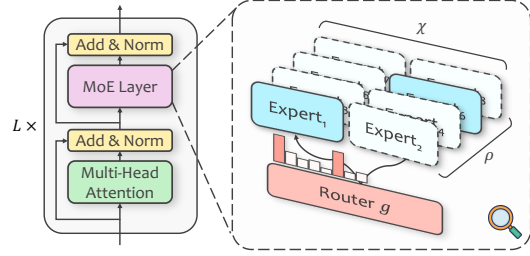


Figure 2. Overview of the MoE layer, where a router selects a sparse subset of experts for each input token, and the granularity χ and expansion ratio ρ determine the expert configuration.

4.2. Mixture-of-Experts (MoE)

The MoE architecture (Shazeer et al., 2017) replaces the dense FFN in the Transformer with multiple experts, activating only a small subset per input to enable conditional computation. An MoE layer consists of N_{expert} independent experts $\{e_i\}_{i=1}^{N_{\text{expert}}}$ and a router $g : \mathbb{R}^{D_{\text{model}}} \rightarrow \mathbb{R}^{N_{\text{expert}}}$. Given a token representation \mathbf{x} , the MoE output is defined as:

$$\text{MoE}(\mathbf{x}) = \sum_{i=1}^{N_{\text{expert}}} g(\mathbf{x})_i e_i(\mathbf{x}). \quad (18)$$

Each expert e_i is a two-layer MLP identical in form to the standard FFN:

$$e_i(\mathbf{x}) = \mathbf{W}_2^i \phi(\mathbf{W}_1^i \mathbf{x} + \mathbf{b}_1^i) + \mathbf{b}_2^i, \quad (19)$$

where the expert parameters are $\mathbf{W}_1^i \in \mathbb{R}^{D_{\text{expert}} \times D_{\text{model}}}$, $\mathbf{b}_1^i \in \mathbb{R}^{D_{\text{expert}}}$, $\mathbf{W}_2^i \in \mathbb{R}^{D_{\text{model}} \times D_{\text{expert}}}$, $\mathbf{b}_2^i \in \mathbb{R}^{D_{\text{model}}}$. The choices of D_{expert} and N_{expert} are discussed in Section 4.4.

4.3. Router

The router g determines which experts are activated by assigning a routing weight $g(\mathbf{x})_i$ to each expert e_i , conditioned on the input \mathbf{x} . It is typically implemented as a linear projection $\mathbf{W}_g \in \mathbb{R}^{N_{\text{expert}} \times D_{\text{model}}}$, and its basic operation is

$$g(\mathbf{x}) = \text{TOP}_k(\text{softmax}(\mathbf{W}_g \mathbf{x})). \quad (20)$$

The softmax produces routing scores over all experts, and $\text{TOP}_k(\cdot)$ selects the top- k experts to enable sparse routing. Thus, the input \mathbf{x} is forwarded only to these selected experts. The router does not transform the input feature, instead, it outputs a control signal that governs expert selection. To prevent excessive load concentration on a small subset of experts (Zhou et al., 2022; Lewis et al., 2021), auxiliary routing losses are commonly used during training (Lepikhin et al., 2021; Fedus et al., 2022). The specific auxiliary losses adopted in our framework are detailed in Section F.

4.4. Granularity

Granularity (χ) and expansion ratio (ρ) are hyperparameters that control the structural decomposition of an MoE layer and its overall parameter capacity (Ludziejewski et al., 2024). The granularity χ specifies how the hidden dimension of the FFN, D_{ffn} , is partitioned across experts:

$$\chi = \frac{D_{\text{ffn}}}{D_{\text{expert}}}. \quad (21)$$

The expansion ratio ρ denotes the parameter increase of the MoE layer relative to a single FFN:

$$\rho = \frac{P_{\text{moe}}}{P_{\text{ffn}}}, \quad (22)$$

where P_{moe} counts the parameter of all experts (excluding the router), and P_{ffn} is that of an FFN with the same architecture. The total number of experts is $N_{\text{expert}} = \chi \cdot \rho$, determined by granularity and expansion ratio.

5. S3: A Modular and Structured Approach to Multimodal Representation Learning

To realize the structured representation principles outlined in Section 3, we introduce S3, a three-stage framework for MMRL. Our goal is to construct representations that are *Task-Sufficient* and *Information-Minimal*, while also satisfying the structural constraints of *latent concept decomposition* and *Distributional Semantic Coherence*. S3 builds on modality-specific MoE encoders that decompose inputs into expert-organized semantic representations, where each subspace corresponds to a distinct latent concept. Each expert specializes in a distinct semantic factor, enabling structural disentanglement. A lightweight router then selectively activates a subset of experts per input by identifying task-relevant semantic components. The following subsections detail each stage of the S3 framework: Specialization, Selection, and Sparsification.

5.1. Expert Pretraining for Specialization

The goal of the Specialization stage is to construct a latent space that serves as the semantic basis for task-adaptive routing. This space should be semantically expressive and structurally coherent, organizing recurring semantic factors across modalities while preserving modality-specific details. To this end, we pretrain modality-specific MoE encoders (f^1, f^2) to decompose inputs into concept-level representations distributed across expert-specific subspaces $\{\mathcal{Z}_c\}_{c \in \mathcal{C}}$. This structure enables the model to disentangle multimodal signals into modular semantic units, forming a compositional basis from which task-relevant information can later be selectively extracted.

Optimization Objective. To realize this structured latent space, we formulate the pretraining objective to maximize semantic coverage within each modality while ensuring Distributional Semantic Coherence across modalities:

$$\max_{f^1, f^2} [I(Z^1; X^1) + I(Z^2; X^2)], \quad \text{s.t. DSC.} \quad (23)$$

Here, maximizing mutual information encourages each encoder to preserve rich semantics for each modality, while the DSC constraint in Equation (16) enforces concept-wise cross-modal alignment.

Training Loss Formulation. Directly computing the mutual information in Equation (23) is intractable, so we approximate its variational lower bound using InfoNCE (van den Oord et al., 2018). For a sample x_i^m , the encoder output is $z_i^m = f^m(x_i^m)$, and for any modality pair $(m, \bar{m}) \in \mathcal{M} \times \mathcal{M}$, the InfoNCE objective is:

$$\mathcal{L}_{\text{InfoNCE}}^{[m \rightarrow \bar{m}]} = -\mathbb{E}_i \left[\log \frac{\exp(\langle z_i^m, z_i^{\bar{m}} \rangle / \tau)}{\sum_j \exp(\langle z_i^m, z_j^{\bar{m}} \rangle / \tau)} \right], \quad (24)$$

where $\langle \cdot, \cdot \rangle$ denotes ℓ_2 -normalized cosine similarity and τ is the temperature. To satisfy the objective Equation (23), we employ three loss components. \mathcal{L}_{rep} maximizes $I(X^m; Z^m)$ by encouraging each encoder to preserve rich and diverse semantic factors within its modality:

$$\mathcal{L}_{\text{rep}} = \frac{1}{2} \left(\mathcal{L}_{\text{InfoNCE}}^{[1 \rightarrow 1]} + \mathcal{L}_{\text{InfoNCE}}^{[2 \rightarrow 2]} \right). \quad (25)$$

The hard DSC constraint is accounted for by \mathcal{L}_{dsc} , which encourages samples that share the same latent concept to occupy nearby regions across modalities:

$$\mathcal{L}_{\text{dsc}} = \frac{1}{2} \left(\mathcal{L}_{\text{InfoNCE}}^{[1 \rightarrow 2]} + \mathcal{L}_{\text{InfoNCE}}^{[2 \rightarrow 1]} \right). \quad (26)$$

Although InfoNCE is computed at the instance level, its contrastive signal implicitly shapes the expert-wise activation patterns, promoting distributional alignment of semantically shared concepts across modalities.

\mathcal{L}_{aux} regularizes the router g by encouraging balanced expert utilization across the data distribution and promoting confident, input-conditioned expert activation. This prevents expert collapse and facilitates semantic specialization by distributing distinct features across experts. A detailed formulation is provided in Section F. The final training objective for Specialization is the weighted sum:

$$\mathcal{L}_{\text{special}} = \lambda_{\text{rep}} \mathcal{L}_{\text{rep}} + \lambda_{\text{dsc}} \mathcal{L}_{\text{dsc}} + \lambda_{\text{aux}} \mathcal{L}_{\text{aux}}. \quad (27)$$

5.2. Router-Only Task Adaptation for Expert Selection

A central challenge in task adaptation is to determine how to selectively access semantically meaningful components of the pretrained latent space based on task demands. Unlike conventional supervised learning, which jointly updates both encoders and classifiers (Ma et al., 2018; liang et al., 2022), our approach takes a structurally constrained path: we freeze all pretrained experts and attention modules, and fine-tune only the lightweight router g , which accounts for a negligible fraction of the total parameters (Section H.3). Rather than modifying the latent space, the router adaptively controls access to it, enabling task-specific selection over semantic components.

This is nontrivial because task relevance is inherently context-dependent: even for the same input, the required semantics may differ across tasks. Instead of explicitly defining task-relevant features, we leverage class labels as

weak supervision, treating them as proxies for semantic consistency. We assume that label-consistent samples are likely to express common latent factors essential for the task. Accordingly, the router is trained to maximize mutual information among label-consistent samples, encouraging it to route inputs through experts that capture task-relevant semantics.

Optimization Objective. To formalize the goal of task-driven routing, we define an objective that reflects the two principles introduced in Section 3.1. The aim is to construct routed representations (Z_Y^1, Z_Y^2) that approximate the optimal task-specific representations (Z_Y^{1*}, Z_Y^{2*}) , by encouraging them to retain task-relevant information while discarding task-irrelevant details from the input. Formally, we express this as the following objective, where α balances the two terms:

$$\max_g \left[\underbrace{I(Z_Y^1, Z_Y^2; Y)}_{\text{Task-Sufficiency}} - \alpha \cdot \underbrace{I(Z_Y^1, Z_Y^2; X^1, X^2|Y)}_{\text{Information-Minimality}} \right]. \quad (28)$$

Training Loss Formulation. Direct computation of Equation (28) is intractable, so we approximate each term using variational objectives that operationalize our design objective: the router should learn to activate experts that respond to task-relevant latent factors in the input, while suppressing task-irrelevant variations. To approximate the Task-Sufficiency term, we adopt the supervised contrastive (SupCon) loss (Khosla et al., 2020), originally introduced to enforce alignment between positive pairs defined by class labels. In our framework, we reinterpret SupCon as a mechanism to maximize mutual information among label-consistent representations. For a sample x_i^m with positive index set $\mathcal{S}_{y_i} = \{s \mid y_s = y_i\}$, the SupCon loss is:

$$\mathcal{L}_{\text{SupCon}}^{[m \rightarrow \bar{m}]} = -\mathbb{E}_i \mathbb{E}_s \left[\log \frac{\exp(\langle z_i^m, z_s^{\bar{m}} \rangle / \tau)}{\sum_j \exp(\langle z_i^m, z_j^{\bar{m}} \rangle / \tau)} \right]. \quad (29)$$

We show in Section E.2 that this loss provides a valid lower bound on task-conditioned mutual information. The final Task-Sufficiency loss averages over all four inter- and intra-modal directions:

$$\mathcal{L}_{\text{suff}} = \frac{1}{4} \sum_{m, \bar{m}} \mathcal{L}_{\text{SupCon}}^{[m \rightarrow \bar{m}]} \quad (30)$$

To estimate the Information-Minimality term, we consider its expression as a KL divergence $I(Z; X|Y) = \mathbb{E}_{p(x,y)} [D_{\text{KL}}(p(z|x) \| p(z|y))]$. We approximate both conditional distributions using von Mises-Fisher (vMF) distributions, leveraging the fact that, during the Specialization stage, encoder outputs lie on the unit hypersphere due to InfoNCE normalization. Specifically, $p(z|x)$ is modeled as a vMF distribution centered at the instance representation $\mu_x = f(x)$, while $p(z|y)$ is modeled using the mean of label-consistent representations in the batch, $\hat{\mu}_y = \frac{\mu_y}{\|\mu_y\|}$, where $\mu_y = \frac{1}{|\mathcal{S}_y|} \sum_{s \in \mathcal{S}_y} z_s$. Under the equal concentration

assumption ($\kappa_x = \kappa_y$), the KL divergence reduces to an inner product form, yielding the following compactness loss:

$$\mathcal{L}_{\text{Comp}}^{[m \rightarrow \bar{m}]} = -\mathbb{E}_{p(x^m, y)} [\langle \mu_x^m, \hat{\mu}_y^{\bar{m}} \rangle]. \quad (31)$$

Averaging across modality pairs gives the Information-Minimality loss:

$$\mathcal{L}_{\text{min}} = \frac{1}{4} \sum_{m, \bar{m}} \mathcal{L}_{\text{Comp}}^{[m \rightarrow \bar{m}]} \quad (32)$$

The final objective for the Selection stage is a weighted sum:

$$\mathcal{L}_{\text{select.}} = \lambda_{\text{suff}} \mathcal{L}_{\text{suff}} + \lambda_{\text{min}} \mathcal{L}_{\text{min}} \quad (33)$$

Unlike Specialization, this stage does not include auxiliary routing losses, since the objective is not to balance expert usage but to selectively activate experts that are relevant to the target task. A complete derivation of the Information-Minimality estimator is provided in Section E.3.

5.3. Inference-Time Pruning for Sparsification

The final stage of the S3 framework, Sparsification, aims to make the representation more efficient at inference time. In the previous Selection stage, the router was optimized to favor experts whose activations yield more task-relevant representations, implicitly assigning higher scores to those more informative for downstream prediction. Consequently, the routing scores can be interpreted as quantitative indicators of each input-expert pair’s contribution to the task. However, conventional MoE layers activate a fixed number of experts (e.g., top- k) per input, regardless of their actual utility. This can lead to redundant computation and allow irrelevant experts to contribute.

To mitigate this, we introduce an inference-time pruning procedure that requires no additional training. For a given batch, we collect the top- k routing scores for all input-expert pairs and sort them. We then retain only the top $p \in [0, 1]$ proportion of pairs, referred to as the *preservation ratio*, and prune the remaining $(1 - p)$ proportion from computation. Since residual connections remain active, removing a routing path does not completely sever the overall flow of information.

Expected Behavior. Sparsification effectively regulates the amount of information retained in the representation by adjusting the preservation ratio p . As p gradually decreases from 1 to 0, we expect downstream performance to follow a reverse U-shaped trend, the characteristic pruning curve:

1. **Task-Irrelevant Pruning.** At high p values, pruning removes predominantly task-irrelevant paths, yielding a cleaner representation. As a result, performance typically improves or remains the same as when $p = 1$.
2. **Optimal Sparsity Regime (Sweet Spot).** At an appropriate sparsity level, unnecessary information is removed while task-relevant routes remain intact. The representation becomes minimal yet still sufficient, and performance reaches its peak.

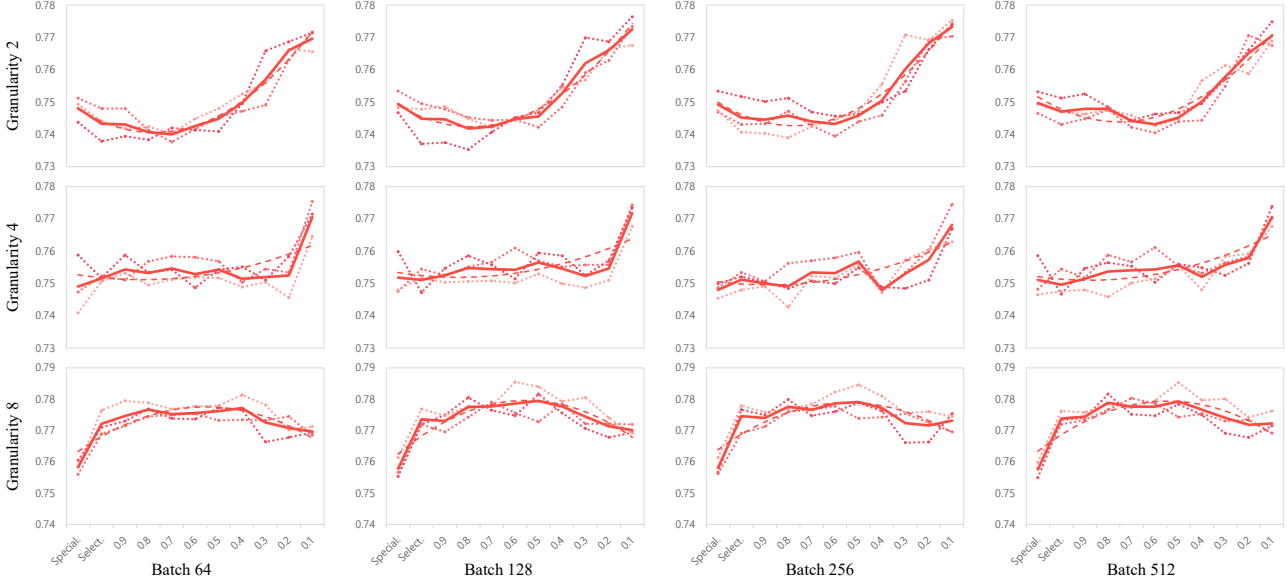


Figure 3. Performance on MOSEI across batch sizes (64-512) and χ (2,4,8). Dotted lines show individual random seeds, the dashed line their trend, and the solid line the mean. All results follow our three-stage pipeline, with p decreased progressively during Sparsification.

- Over-Pruning.** When p becomes too small, pruning begins to remove task-relevant routes, discarding essential information and causing performance degradation.

6. Experiments

We evaluate our method on four multimodal benchmarks from the MultiBench (Liang et al., 2021), following its standardized evaluation protocol: MOSEI (Bagher Zadeh et al., 2018), MOSI (Zadeh et al., 2016), UR-FUNNY (Hasan et al., 2019), and MUSTARD (Castro et al., 2019). We compare S3 against representative baselines from three families: (1) Contrastive learning (CLIP (Radford et al., 2021)); (2) InfoMax-based approaches (FOCAL (Liu et al., 2023), DisentangledSSL (Wang et al., 2025), JointOpt (Pan et al., 2021)); (3) Augmentation-driven methods (FactorCL (Liang et al., 2023)). Following Wang et al. (2025), we report linear probing accuracy, averaged over three random seeds.

Since MoE architectures inherently introduce a larger total parameter budget than dense models, we follow prior works (Jiang et al., 2024; Ludziejewski et al., 2024) and control for the *active parameters*, those directly participating in token-wise transformations (attention and expert modules, excluding the router), for a fair comparison. Specifically, we set the top- k value equal to the granularity ($k = \chi$) in each experiment, so that the number of activated expert parameters per token matches that of the original FFN.

6.1. Analysis of S3 Stages on MOSEI

We analyze how each stage of S3 influences downstream performance using MOSEI, the largest benchmark in our evaluation suite. As shown in Figure 3, the pruning curves exhibit consistent trends across different batch sizes (64–512), while their shapes vary substantially with the chosen gran-

ularity. This suggests that the performance dynamics are governed more by the structural properties of the representation than by training configurations.

At low granularity ($\chi = 2$), the FFN is decomposed into a small number of large experts, causing multiple semantic concepts to be entangled within each expert. Such high degree of entanglement introduces routing ambiguity, making it difficult for the router to reliably identify task-relevant experts. Consequently, performance degrades during Selection and early Sparsification, exhibiting a delayed U-shaped trend where performance recovers only after pruning removes enough noise that the remaining pathways carry a cleaner signal.

In contrast, high granularity ($\chi = 8$) divides the FFN into many small experts, yielding a finer expert-level separation of semantic concepts. In this setting, the router can more reliably assign high scores to task-relevant experts, allowing early pruning to effectively remove task-irrelevant paths. As a result, performance improves initially, peaks at an optimal sparsity level, and declines only when pruning begins to discard essential task-relevant routes, consistent with the characteristic reverse U-shaped pattern hypothesized in Section 5.3. The intermediate setting ($\chi = 4$) exhibits behavior between these two extremes, with smoother performance transitions across pruning ratios.

6.2. Benchmark-Wide Evaluation of the S3 Framework

Table 1 summarizes the performance progression of S3 across the four multimodal benchmarks. Despite differences in task characteristics and dataset scales, the structural pruning patterns analyzed in Section 6.1 consistently recur across all benchmarks.

With sufficiently high granularity, all benchmarks exhibit a

Toward Structural Multimodal Representations: Specialization, Selection, and Sparsification via Mixture-of-Experts

DATASET	χ	Special.	Select.	0.9	0.8	0.7	0.6	0.5	0.4	0.3	0.2	0.1
MOSEI	2	74.94(0.35)	74.48(0.68)	74.46(0.62)	74.18(0.56)	74.24(0.18)	74.47(0.04)	74.55(0.29)	75.27(0.37)	76.20(0.70)	76.60(0.29)	77.25(0.45)
	4	75.18(0.70)	75.11(0.37)	75.25(0.22)	75.48(0.40)	75.44(0.31)	75.42(0.59)	75.65(0.33)	75.45(0.43)	75.23(0.36)	75.46(0.32)	77.18(0.36)
	8	75.78(0.32)	77.36(0.29)	77.31(0.30)	77.75(0.31)	77.77(0.13)	77.86(0.60)	77.95(0.59)	77.77(0.19)	77.44(0.53)	77.13(0.32)	77.01(0.16)
MOSI	2	59.86(0.59)	59.77(1.72)	60.06(0.81)	59.33(1.14)	58.84(0.30)	59.96(0.45)	60.25(1.68)	61.42(0.99)	62.15(3.67)	61.56(1.09)	64.82(1.85)
	4	62.76(0.81)	63.85(2.41)	63.48(1.35)	62.03(1.26)	63.70(0.55)	64.43(2.10)	65.45(1.90)	63.41(1.24)	64.43(2.24)	63.78(1.74)	64.80(2.27)
	8	63.56(2.18)	64.29(1.27)	64.38(0.30)	65.16(0.25)	66.13(0.51)	65.55(1.40)	65.60(1.31)	65.16(1.41)	65.60(1.79)	65.99(0.55)	65.01(1.39)
UR-FUNNY	2	62.79(1.10)	62.85(1.00)	62.10(0.71)	62.13(0.80)	61.94(1.28)	62.67(1.37)	62.89(1.05)	62.51(0.99)	62.51(0.95)	62.92(1.67)	64.46(0.76)
	4	63.17(0.72)	64.18(0.99)	64.34(1.42)	64.02(0.72)	64.52(0.58)	64.49(0.60)	64.11(0.86)	64.74(0.74)	64.11(0.61)	64.05(0.47)	62.89(0.80)
	8	63.61(0.49)	63.52(0.62)	63.58(0.66)	63.55(0.36)	63.48(0.24)	63.93(0.77)	63.52(0.19)	64.40(0.72)	64.68(0.96)	64.87(0.63)	63.48(1.13)
MUSTARD	2	57.49(3.57)	57.49(3.02)	58.45(1.51)	56.28(2.93)	60.14(6.91)	58.70(6.91)	58.94(6.03)	57.73(4.66)	60.63(5.86)	60.14(0.00)	61.35(3.99)
	4	56.76(3.57)	57.73(3.42)	57.00(2.54)	61.35(1.51)	58.45(2.93)	58.45(3.35)	58.94(2.33)	57.97(5.02)	56.52(5.07)	53.14(2.93)	53.14(5.81)
	8	58.70(3.16)	61.59(0.72)	61.84(0.84)	62.56(1.11)	61.84(1.11)	60.87(0.72)	61.11(1.11)	60.63(1.51)	61.59(1.45)	58.45(0.84)	59.18(4.82)

Table 1. Prediction accuracy (%) of the S3 framework across benchmarks and granularities, covering Specialization, Selection, and Sparsification (evaluated over preservation ratios). All results are averaged over three random seeds with standard deviations.

monotonic performance improvement from Specialization to Selection, reaching peak performance during Sparsification. This consistency demonstrates that the benefits of fine-grained semantic decomposition and router-based information refinement are not benchmark-specific artifacts, but rather stem from the intrinsic inductive advantages of the S3 architecture. Conversely, low-granularity settings exhibit similar degradation during Selection and early instability in Sparsification, indicating that coarse-grained decomposition leads to less stable performance dynamics.

Beyond these architectural effects, we also observe that the scale of the dataset strongly influences training stability. Larger datasets such as MOSEI and UR-FUNNY exhibit minimal variance across random seeds, whereas variance is substantially higher for smaller datasets such as MOSI and MUSTARD. This effect is most notable at $\chi = 2$, where limited data and coarse decomposition jointly lead to more variable routing behavior.

6.3. Comparison with Prior Methods

As shown in Table 2, the S3 framework consistently outperforms a broad range of prior methods, spanning contrastive learning, InfoMax-based, and augmentation-driven approaches. DisentangledSSL, which builds on an information-theoretic analysis of MMRL via the InfoMax principle, performs competitively across all benchmarks. However, it is consistently outperformed by S3, highlighting the benefits of our structured approach. These gains stem from S3’s ability to satisfy the two criteria at the core of our formulation, Task-Sufficiency and Information-Minimality.

The Specialization stage aims to retain a rich set of semantic factors. However, our results show that preserving more information alone does not necessarily guarantee improved downstream performance. In contrast, the Selection stage employs a router to activate task-relevant semantic experts, addressing both the shared-only limitation of contrastive learning and the indiscriminate retention of InfoMax methods. The most significant improvements arise in the Sparsification stage, where pruning low-contribution path-

	MOSEI	MOSI	UR-FUNNY	MUSTARD
CLIP	76.87(0.45)	64.24(0.88)	62.73(0.92)	56.04(4.19)
FactorCL-emb	71.80(0.64)	62.97(0.81)	63.29(2.07)	56.76(4.66)
FactorCL-proj	74.61(1.65)	56.02(1.26)	61.25(0.47)	55.80(2.18)
FOCAL	76.77(0.51)	63.65(1.09)	63.17(0.96)	58.21(2.21)
JointOpt	76.71(0.14)	65.02(1.96)	63.58(1.45)	57.73(4.12)
DisentangledSSL	77.45(0.06)	65.16(0.81)	64.24(1.54)	61.60(2.61)
Specialization	75.78(0.32)	63.56(2.18)	63.61(0.49)	58.70(3.16)
+ Selection	77.36(0.29)	64.29(1.27)	63.52(0.62)	61.59(0.72)
+ Sparsification	77.95(0.95)	66.13(0.51)	64.87(0.63)	62.56(1.11)

Table 2. Prediction accuracy (%) on four benchmarks, averaged over three random seeds, with standard deviations. We compare S3 against representative prior methods.

ways sharpens the representation without modifying the underlying encoders. This refinement is not merely for computational efficiency; but introduces a finer-grained, sample-level pruning that complements the task-level routing of the Selection stage, providing a structural advantage unique to S3 and absent from prior methods.

Similarly, augmentation-based methods aim to capture task-relevant features by assuming that they remain invariant across augmented views, while allowing task-irrelevant factors to vary. However, their effectiveness is highly sensitive to the choice of augmentation strategies and often fluctuates across benchmarks. In contrast, S3 achieves stable and reproducible gains without relying on such heuristics, instead using expert routing to structurally disentangle latent semantic factors and selectively recombine them.

7. Conclusion

This work advocates a structural perspective on MMRL. Rather than compressing heterogeneous signals into monolithic embeddings, we emphasize the need to decompose inputs into semantically coherent components, selectively retain task-relevant information, and discard redundant variability. We realize this principle through S3, a three-stage MoE-based framework that progressively specializes, selects, and sparsifies multimodal representations. Empirically, S3 consistently improves performance across diverse benchmarks while exhibiting stable and predictable behav-

ior across semantic granularities and dataset scales. These results suggest that S3’s effectiveness is not merely a result of objective tuning, but of structural inductive biases aligned with the compositional nature of multimodal semantics.

Looking ahead, this structural paradigm opens several promising research directions: (1) modality-adaptive information preservation for task-critical modalities; (2) layer-adaptive modeling of semantic abstraction across model depth; (3) self-supervised routing adaptation to reduce label dependence; (4) enhanced expert specialization for more precise semantic decomposition; and (5) adaptive sparsification with learnable granularity and pruning policies.

Acknowledgements

This work was supported by the Korean Government through the grants from IITP (RS-2021-II211343, RS-2022-II220953, RS-2025-25442338).

Impact Statement

This paper presents work whose goal is to advance the field of Machine Learning. There are many potential societal consequences of our work, none which we feel must be specifically highlighted here.

References

- Almudévar, A., Hernández-Lobato, J. M., Khurana, S., Marxer, R., and Ortega, A. Aligning multimodal representations through an information bottleneck. In *Forty-second International Conference on Machine Learning*, 2025. URL <https://openreview.net/forum?id=zltxOTETfm>.
- Arandjelovic, R. and Zisserman, A. Look, listen and learn. In *Proceedings of the IEEE international conference on computer vision*, pp. 609–617, 2017.
- Bachman, P., Hjelm, R. D., and Buchwalter, W. Learning representations by maximizing mutual information across views. *Advances in neural information processing systems*, 32, 2019.
- Bagher Zadeh, A., Liang, P. P., Poria, S., Cambria, E., and Morency, L.-P. Multimodal language analysis in the wild: CMU-MOSEI dataset and interpretable dynamic fusion graph. In Gurevych, I. and Miyao, Y. (eds.), *Proceedings of the 56th Annual Meeting of the Association for Computational Linguistics (Volume 1: Long Papers)*, pp. 2236–2246, Melbourne, Australia, July 2018. Association for Computational Linguistics. doi: 10.18653/v1/P18-1208. URL <https://aclanthology.org/P18-1208/>.
- Bian, S., Pan, X., Zhao, W. X., Wang, J., Wang, C., and Wen, J.-R. Multi-modal mixture of experts representation learning for sequential recommendation. In *Proceedings of the 32nd ACM International Conference on Information and Knowledge Management, CIKM ’23*, pp. 110–119, New York, NY, USA, 2023. Association for Computing Machinery. ISBN 9798400701245. doi: 10.1145/3583780.3614978. URL <https://doi.org/10.1145/3583780.3614978>.
- Bricken, T., Templeton, A., Batson, J., Chen, B., Jermyn, A., Conerly, T., Turner, N., Anil, C., Denison, C., Askell, A., Lasenby, R., Wu, Y., Kravec, S., Schiefer, N., Maxwell, T., Joseph, N., Hatfield-Dodds, Z., Tamkin, A., Nguyen, K., McLean, B., Burke, J. E., Hume, T., Carter, S., Henighan, T., and Olah, C. Towards monosemanticity: Decomposing language models with dictionary learning. *Transformer Circuits Thread*, 2023. <https://transformer-circuits.pub/2023/monosemantic-features/index.html>.
- Castro, S., Hazarika, D., Pérez-Rosas, V., Zimmermann, R., Mihalcea, R., and Poria, S. Towards multimodal sarcasm detection (an ‘Obviously’ perfect paper). In Korhonen, A., Traum, D., and Màrquez, L. (eds.), *Proceedings of the 57th Annual Meeting of the Association for Computational Linguistics*, pp. 4619–4629, Florence, Italy, July 2019. Association for Computational Linguistics. doi: 10.18653/v1/P19-1455. URL <https://aclanthology.org/P19-1455/>.
- Chen, T., Chen, X., Du, X., Rashwan, A., Yang, F., Chen, H., Wang, Z., and Li, Y. Adamv-moe: Adaptive multi-task vision mixture-of-experts. In *Proceedings of the IEEE/CVF International Conference on Computer Vision (ICCV)*, pp. 17346–17357, October 2023.
- Cherti, M., Beaumont, R., Wightman, R., Wortsman, M., Ilharco, G., Gordon, C., Schuhmann, C., Schmidt, L., and Jitsev, J. Reproducible scaling laws for contrastive language-image learning. In *Proceedings of the IEEE/CVF conference on computer vision and pattern recognition*, pp. 2818–2829, 2023.
- Choi, H., Lee, J., and Kwak, N. What’s making that sound right now? video-centric audio-visual localization. In *Proceedings of the IEEE/CVF International Conference on Computer Vision (ICCV)*, pp. 20095–20104, October 2025.
- Dong, H., Nejjar, I., Sun, H., Chatzi, E., and Fink, O. Simmdg: A simple and effective framework for multi-modal domain generalization. *Advances in Neural Information Processing Systems*, 36:78674–78695, 2023.
- Du, N., Huang, Y., Dai, A. M., Tong, S., Lepikhin, D., Xu, Y., Krikun, M., Zhou, Y., Yu, A. W., Firat, O., et al. Glam:

- Efficient scaling of language models with mixture-of-experts. In *International conference on machine learning*, pp. 5547–5569. PMLR, 2022.
- Ernst, M. O. and Bühlhoff, H. H. Merging the senses into a robust percept. *Trends in Cognitive Sciences*, 8(4):162–169, 2004. ISSN 1364-6613. doi: <https://doi.org/10.1016/j.tics.2004.02.002>. URL <https://www.sciencedirect.com/science/article/pii/S1364661304000385>.
- Fedus, W., Zoph, B., and Shazeer, N. Switch transformers: Scaling to trillion parameter models with simple and efficient sparsity. *Journal of Machine Learning Research*, 23(120):1–39, 2022.
- Ghazanfar, A. A. and Schroeder, C. E. Is neocortex essentially multisensory? *Trends in Cognitive Sciences*, 10(6):278–285, 2006. ISSN 1364-6613. doi: <https://doi.org/10.1016/j.tics.2006.04.008>. URL <https://www.sciencedirect.com/science/article/pii/S1364661306001045>.
- Girdhar, R., El-Nouby, A., Liu, Z., Singh, M., Alwala, K. V., Joulin, A., and Misra, I. Imagebind: One embedding space to bind them all. In *Proceedings of the IEEE/CVF conference on computer vision and pattern recognition*, pp. 15180–15190, 2023.
- Han, X., Nguyen, H., Harris, C. W., Ho, N., and Saria, S. Fusemoe: Mixture-of-experts transformers for fleximodal fusion. In *The Thirty-eighth Annual Conference on Neural Information Processing Systems*, 2024. URL <https://openreview.net/forum?id=jfE7XCE89y>.
- Hasan, M. K., Rahman, W., Bagher Zadeh, A., Zhong, J., Tanveer, M. I., Morency, L.-P., and Hoque, M. E. UR-FUNNY: A multimodal language dataset for understanding humor. In Inui, K., Jiang, J., Ng, V., and Wan, X. (eds.), *Proceedings of the 2019 Conference on Empirical Methods in Natural Language Processing and the 9th International Joint Conference on Natural Language Processing (EMNLP-IJCNLP)*, pp. 2046–2056, Hong Kong, China, November 2019. Association for Computational Linguistics. doi: 10.18653/v1/D19-1211. URL <https://aclanthology.org/D19-1211/>.
- Hjelm, R. D., Fedorov, A., Lavoie-Marchildon, S., Grewal, K., Bachman, P., Trischler, A., and Bengio, Y. Learning deep representations by mutual information estimation and maximization. In *International Conference on Learning Representations*, 2019. URL <https://openreview.net/forum?id=Bk1r3j0cKX>.
- Huai, T., Zhou, J., Wu, X., Chen, Q., Bai, Q., Zhou, Z., and He, L. Cl-moe: Enhancing multimodal large language model with dual momentum mixture-of-experts for continual visual question answering. In *Proceedings of the Computer Vision and Pattern Recognition Conference*, pp. 19608–19617, 2025.
- Huben, R., Cunningham, H., Smith, L. R., Ewart, A., and Sharkey, L. Sparse autoencoders find highly interpretable features in language models. In *The Twelfth International Conference on Learning Representations*, 2024. URL <https://openreview.net/forum?id=F76bwrSLeK>.
- Jia, C., Yang, Y., Xia, Y., Chen, Y.-T., Parekh, Z., Pham, H., Le, Q., Sung, Y.-H., Li, Z., and Duerig, T. Scaling up visual and vision-language representation learning with noisy text supervision. In *International conference on machine learning*, pp. 4904–4916. PMLR, 2021.
- Jiang, A. Q., Sablayrolles, A., Roux, A., Mensch, A., Savary, B., Bamford, C., Chaplot, D. S., Casas, D. d. l., Hanna, E. B., Bressand, F., et al. Mixtral of experts. *arXiv preprint arXiv:2401.04088*, 2024.
- Jiang, Q., Chen, C., Zhao, H., Chen, L., Ping, Q., Tran, S. D., Xu, Y., Zeng, B., and Chilimbi, T. Understanding and constructing latent modality structures in multi-modal representation learning. In *Proceedings of the IEEE/CVF Conference on Computer Vision and Pattern Recognition*, pp. 7661–7671, 2023.
- Johnson, A., Pollard, T., and Mark, R. MIMIC-III Clinical Database. *PhysioNet*, September 2016. doi: 10.13026/C2XW26. URL <https://doi.org/10.13026/C2XW26>. Version 1.4.
- Khan, A., Asmatullah, L., Malik, A., Khan, S., and Asif, H. A survey on self-supervised contrastive learning for multimodal text-image analysis. *arXiv preprint arXiv:2503.11101*, 2025.
- Khosla, P., Teterwak, P., Wang, C., Sarna, A., Tian, Y., Isola, P., Maschinot, A., Liu, C., and Krishnan, D. Supervised contrastive learning. *Advances in neural information processing systems*, 33:18661–18673, 2020.
- Lee, M. and Pavlovic, V. Private-shared disentangled multimodal vae for learning of latent representations. In *2021 IEEE/CVF Conference on Computer Vision and Pattern Recognition Workshops (CVPRW)*, pp. 1692–1700, 2021. doi: 10.1109/CVPRW53098.2021.00185.
- Lepikhin, D., Lee, H., Xu, Y., Chen, D., Firat, O., Huang, Y., Krikun, M., Shazeer, N., and Chen, Z. {GS}hard: Scaling giant models with conditional computation and automatic sharding. In *International Conference on Learning Representations*, 2021. URL <https://openreview.net/forum?id=qrwe7XHTmYb>.

- Lewis, M., Bhosale, S., Dettmers, T., Goyal, N., and Zettlemoyer, L. Base layers: Simplifying training of large, sparse models. In *International Conference on Machine Learning*, pp. 6265–6274. PMLR, 2021.
- Li, J., Selvaraju, R., Gotmare, A., Joty, S., Xiong, C., and Hoi, S. C. H. Align before fuse: Vision and language representation learning with momentum distillation. *Advances in neural information processing systems*, 34: 9694–9705, 2021.
- Li, J., Li, D., Xiong, C., and Hoi, S. Blip: Bootstrapping language-image pre-training for unified vision-language understanding and generation. In *International conference on machine learning*, pp. 12888–12900. PMLR, 2022.
- Li, T., Guo, H., Grazioli, F., Gerstein, M., and Min, M. R. Disentangled wasserstein autoencoder for t-cell receptor engineering. In *Thirty-seventh Conference on Neural Information Processing Systems*, 2023. URL <https://openreview.net/forum?id=Eb74zfBkWa>.
- Li, Y., Jiang, S., Hu, B., Wang, L., Zhong, W., Luo, W., Ma, L., and Zhang, M. Uni-moe: Scaling unified multimodal llms with mixture of experts. *IEEE Transactions on Pattern Analysis and Machine Intelligence*, 2025.
- liang, h., Fan, Z., Sarkar, R., Jiang, Z., Chen, T., Zou, K., Cheng, Y., Hao, C., and Wang, Z. M³vit: Mixture-of-experts vision transformer for efficient multi-task learning with model-accelerator co-design. In Koyejo, S., Mohamed, S., Agarwal, A., Belgrave, D., Cho, K., and Oh, A. (eds.), *Advances in Neural Information Processing Systems*, volume 35, pp. 28441–28457. Curran Associates, Inc., 2022.
- Liang, P. P., Lyu, Y., Fan, X., Wu, Z., Cheng, Y., Wu, J., Chen, L., Wu, P., Lee, M. A., Zhu, Y., et al. Multibench: Multiscale benchmarks for multimodal representation learning. *Advances in neural information processing systems*, 2021(DB1):1, 2021.
- Liang, P. P., Deng, Z., Ma, M. Q., Zou, J., Morency, L.-P., and Salakhutdinov, R. Factorized contrastive learning: Going beyond multi-view redundancy. In *Thirty-seventh Conference on Neural Information Processing Systems*, 2023. URL <https://openreview.net/forum?id=allS7EtRJP>.
- Liang, V. W., Zhang, Y., Kwon, Y., Yeung, S., and Zou, J. Y. Mind the gap: Understanding the modality gap in multi-modal contrastive representation learning. *Advances in Neural Information Processing Systems*, 35: 17612–17625, 2022.
- Liao, C., So, C., Tsiligkaridis, T., and Kulis, B. Multimodal unsupervised domain generalization by retrieving across the modality gap. In *The Thirteenth International Conference on Learning Representations*, 2025. URL <https://openreview.net/forum?id=bqoHdVMlbt>.
- Linsker, R. Self-organization in a perceptual network. *Computer*, 21(3):105–117, 1988. doi: 10.1109/2.36.
- Liu, S., Kimura, T., Liu, D., Wang, R., Li, J., Diggavi, S., Srivastava, M., and Abdelzaher, T. Focal: Contrastive learning for multimodal time-series sensing signals in factorized orthogonal latent space. *Advances in Neural Information Processing Systems*, 36:47309–47338, 2023.
- Locatello, F., Bauer, S., Lucic, M., Raetsch, G., Gelly, S., Schölkopf, B., and Bachem, O. Challenging common assumptions in the unsupervised learning of disentangled representations. In *international conference on machine learning*, pp. 4114–4124. PMLR, 2019.
- Ludziejewski, J., Krajewski, J., Adamczewski, K., Pióro, M., Krutul, M., Antoniak, S., Ciebiera, K., Król, K., Odrzygóźdź, T., Sankowski, P., Cygan, M., and Jaszczur, S. Scaling laws for fine-grained mixture of experts. In Salakhutdinov, R., Kolter, Z., Heller, K., Weller, A., Oliver, N., Scarlett, J., and Berkenkamp, F. (eds.), *Proceedings of the 41st International Conference on Machine Learning Research*, volume 235 of *Proceedings of Machine Learning Research*, pp. 33270–33288. PMLR, 21–27 Jul 2024. URL <https://proceedings.mlr.press/v235/ludziejewski24a.html>.
- Ma, J., Zhao, Z., Yi, X., Chen, J., Hong, L., and Chi, E. H. Modeling task relationships in multi-task learning with multi-gate mixture-of-experts. In *Proceedings of the 24th ACM SIGKDD International Conference on Knowledge Discovery & Data Mining, KDD '18*, pp. 1930–1939, New York, NY, USA, 2018. Association for Computing Machinery. ISBN 9781450355520. doi: 10.1145/3219819.3220007. URL <https://doi.org/10.1145/3219819.3220007>.
- Mustafa, B., Riquelme, C., Puigcerver, J., Jenatton, R., and Houlsby, N. Multimodal contrastive learning with limoe: the language-image mixture of experts. *Advances in Neural Information Processing Systems*, 35:9564–9576, 2022.
- Oldfield, J., Im, S., Li, S., Nicolaou, M. A., Patras, I., and Chrysos, G. G. Towards interpretability without sacrifice: Faithful dense layer decomposition with mixture of decoders. *arXiv preprint arXiv:2505.21364*, 2025.
- Pan, Z., Niu, L., Zhang, J., and Zhang, L. Disentangled information bottleneck. In *Proceedings of the AAAI Conference on Artificial Intelligence*, volume 35, pp. 9285–9293, 2021.

- Park, J., Jin, A. Y., Kim, K.-E., and Kang, J. Monet: Mixture of monosemantic experts for transformers. In *The Thirteenth International Conference on Learning Representations*, 2025. URL <https://openreview.net/forum?id=1Ogw1SHY3p>.
- Park, S., Lee, M., Kang, J., Choi, H., Park, Y., Cho, J., Lee, A., and Kim, D. VLaad: Vision and language assistant for autonomous driving. In *Proceedings of the IEEE/CVF Winter Conference on Applications of Computer Vision (WACV) Workshops*, pp. 980–987, January 2024.
- Poole, B., Sun, C., Schmid, C., Krishnan, D., Isola, P., and Tian, Y. What makes for good views for contrastive representation learning? In *NeurIPS 2020*, 2020.
- Radford, A., Narasimhan, K., Salimans, T., and Sutskever, I. Improving language understanding by generative pre-training. *OpenAI*, 2018.
- Radford, A., Kim, J. W., Hallacy, C., Ramesh, A., Goh, G., Agarwal, S., Sastry, G., Askell, A., Mishkin, P., Clark, J., et al. Learning transferable visual models from natural language supervision. In *International conference on machine learning*, pp. 8748–8763. Pmlr, 2021.
- Rae, J. W., Borgeaud, S., Cai, T., Millican, K., Hoffmann, J., Song, F., Aslanides, J., Henderson, S., Ring, R., Young, S., Rutherford, E., Hennigan, T., Menick, J., Cassirer, A., Powell, R., van den Driessche, G., Hendricks, L. A., Rauh, M., Huang, P.-S., Glaese, A., Welbl, J., Dhathathri, S., Huang, S., Uesato, J., Meller, J. F. J., Higgins, I., Creswell, A., McAleese, N., Wu, A., Elsen, E., Jayakumar, S. M., Buchatskaya, E., Budden, D., Sutherland, L., Simonyan, K., Paganini, M., Sifre, L., Martens, L., Li, X. L., Kuncoro, A., Nematzadeh, A., Gribovskaya, E., Donato, D., Lazaridou, A., Mensch, A., Lespiau, J.-B., Tsimpoukelli, M., Grigorev, N. K., Fritz, D., Sottiaux, T., Pajarskas, M., Pohlen, T., Gong, Z., Toyama, D., de Masson d’Autume, C., Li, Y., Terzi, T., Mikulik, V., Babuschkin, I., Clark, A., de Las Casas, D., Guy, A., Jones, C., Bradbury, J., Johnson, M. G., Hechtman, B. A., Weidinger, L., Gabriel, I., Isaac, W. S., Lockhart, E., Osindero, S., Rimell, L., Dyer, C., Vinyals, O., Ayoub, K. W., Stanway, J., Bennett, L. L., Hassabis, D., Kavukcuoglu, K., and Irving, G. Scaling language models: Methods, analysis & insights from training gopher. *ArXiv*, abs/2112.11446, 2021. URL <https://api.semanticscholar.org/CorpusID:245353475>.
- Rajbhandari, S., Li, C., Yao, Z., Zhang, M., Aminabadi, R. Y., Awan, A. A., Rasley, J., and He, Y. DeepSpeed-moe: Advancing mixture-of-experts inference and training to power next-generation ai scale. In *International conference on machine learning*, pp. 18332–18346. PMLR, 2022.
- Riquelme, C., Puigcerver, J., Mustafa, B., Neumann, M., Jenatton, R., Susano Pinto, A., Keyzers, D., and Houlsby, N. Scaling vision with sparse mixture of experts. *Advances in Neural Information Processing Systems*, 34: 8583–8595, 2021.
- Schrodi, S., Hoffmann, D. T., Argus, M., Fischer, V., and Brox, T. Two effects, one trigger: On the modality gap, object bias, and information imbalance in contrastive vision-language models. In *The Thirteenth International Conference on Learning Representations*, 2025. URL <https://openreview.net/forum?id=uAFHCZRmXk>.
- Shazeer, N., Mirhoseini, A., Maziarz, K., Davis, A., Le, Q., Hinton, G., and Dean, J. Outrageously large neural networks: The sparsely-gated mixture-of-experts layer. In *International Conference on Learning Representations*, 2017. URL <https://openreview.net/forum?id=BlckMDqlg>.
- Shen, S., Yao, Z., Li, C., Darrell, T., Keutzer, K., and He, Y. Scaling vision-language models with sparse mixture of experts. In *The 2023 Conference on Empirical Methods in Natural Language Processing*, 2023. URL <https://openreview.net/forum?id=IpJ5rAFLv7>.
- Soatto, S. and Chiuso, A. Visual scene representations: Sufficiency, minimality, invariance and deep approximations. In *International Conference on Learning Representations*, 2014. URL <https://api.semanticscholar.org/CorpusID:85529011>.
- Soatto, S. and Chiuso, A. Visual representations: Defining properties and deep approximation. In *Proceedings of the International Conference on Learning Representations (ICLR)*, June 2016.
- Tian, Y., Krishnan, D., and Isola, P. Contrastive multiview coding. In *European conference on computer vision*, pp. 776–794. Springer, 2020.
- Tishby, N. and Zaslavsky, N. Deep learning and the information bottleneck principle. In *2015 IEEE information theory workshop (itw)*, pp. 1–5. Ieee, 2015.
- Touvron, H., Lavril, T., Izacard, G., Martinet, X., Lachaux, M.-A., Lacroix, T., Rozière, B., Goyal, N., Hambro, E., Azhar, F., Rodriguez, A., Joulin, A., Grave, E., and Lample, G. Llama: Open and efficient foundation language models. *CoRR*, abs/2302.13971, 2023. URL <http://dblp.uni-trier.de/db/journals/corr/corr2302.html#abs-2302-13971>.
- van den Oord, A., Li, Y., and Vinyals, O. Representation learning with contrastive predictive coding. *CoRR*, abs/1807.03748, 2018. URL

<http://dblp.uni-trier.de/db/journals/corr/corr1807.html#abs-1807-03748>.

Vaswani, A., Shazeer, N., Parmar, N., Uszkoreit, J., Jones, L., Gomez, A. N., Kaiser, Ł., and Polosukhin, I. Attention is all you need. *Advances in neural information processing systems*, 30, 2017.

Wang, C., Gupta, S., Zhang, X., Tonekaboni, S., Jegelka, S., Jaakkola, T., and Uhler, C. An information criterion for controlled disentanglement of multimodal data. In *The Thirteenth International Conference on Learning Representations*, 2025. URL <https://openreview.net/forum?id=3n4RY25UWP>.

Yang, X., Venhoff, C., Khakzar, A., de Witt, C. S., Dokania, P. K., Bibi, A., and Torr, P. Mixture of experts made intrinsically interpretable. In *Forty-second International Conference on Machine Learning*, 2025. URL <https://openreview.net/forum?id=6QERrXMLP2>.

Ye, H. and Xu, D. Taskexpert: Dynamically assembling multi-task representations with memorial mixture-of-experts. In *Proceedings of the IEEE/CVF International Conference on Computer Vision (ICCV)*, pp. 21828–21837, October 2023.

Yu, X., Chen, Z., He, Y., Fu, T., Yang, C., Xu, C., Ma, Y., Hu, X., Cao, Z., Xu, J., et al. The latent space: Foundation, evolution, mechanism, ability, and outlook. *arXiv preprint arXiv:2604.02029*, 2026.

Yun, S., Choi, I., Peng, J., Wu, Y., Bao, J., Zhang, Q., Xin, J., Long, Q., and Chen, T. Flex-moe: Modeling arbitrary modality combination via the flexible mixture-of-experts. In Globerson, A., Mackey, L., Belgrave, D., Fan, A., Paquet, U., Tomczak, J., and Zhang, C. (eds.), *Advances in Neural Information Processing Systems*, volume 37, pp. 98782–98805. Curran Associates, Inc., 2024. doi: 10.52202/079017-3135.

Zadeh, A., Zellers, R., Pincus, E., and Morency, L.-P. Mosi: multimodal corpus of sentiment intensity and subjectivity analysis in online opinion videos. *arXiv preprint arXiv:1606.06259*, 2016.

Zhang, X., Shivashankar, G., and Uhler, C. Partially shared multi-modal embedding learns holistic representation of cell state. *bioRxiv*, 2024a. doi: 10.1101/2024.10.01.615977. URL <https://www.biorxiv.org/content/early/2024/10/03/2024.10.01.615977>.

Zhang, Z., Liu, S., Yu, J., Cai, Q., Zhao, X., Zhang, C., Liu, Z., Liu, Q., Zhao, H., Hu, L., Jiang, P., and Gai, K. M3oe: Multi-domain multi-task mixture-of experts recommendation framework. In *Proceedings of the 47th*

International ACM SIGIR Conference on Research and Development in Information Retrieval, SIGIR '24, pp. 893–902, New York, NY, USA, 2024b. Association for Computing Machinery. ISBN 9798400704314. doi: 10.1145/3626772.3657686. URL <https://doi.org/10.1145/3626772.3657686>.

Zhou, Y., Lei, T., Liu, H., Du, N., Huang, Y., Zhao, V., Dai, A. M., Le, Q. V., Laudon, J., et al. Mixture-of-experts with expert choice routing. *Advances in Neural Information Processing Systems*, 35:7103–7114, 2022.

A. Conceptual Overview of Our Framework

Multimodal data inherently contain heterogeneous semantic components, not all of which are equally relevant to the target task. Our core insight is that these semantic components can be decomposed, selectively represented, and filtered in the representation space to achieve Task-Sufficient and Information-Minimal representations. As illustrated in Figure 4, our framework first disentangles the multimodal observation into its underlying semantic constituents. We then map these into a modality-agnostic latent space, where only the components deemed relevant to the task are selectively preserved and activated. This figure provides the conceptual foundation for our method, where the goal is not merely to fuse modalities, but to structurally filter and retain only the minimal sufficient set of features needed for the task at hand. This idea serves as the design principle for our approach S3, motivating our decomposition of multimodal features, expert specialization, and task-driven expert selection via routing.

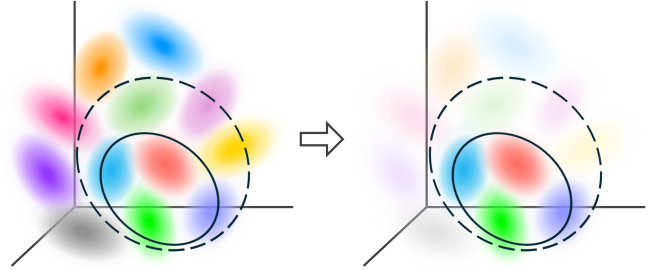


Figure 4. Multimodal observations contain heterogeneous semantic components. Our framework decomposes these components (in different colors) and maps them into a modality-agnostic space, preserving only the task-relevant subset. Dashed ellipses denote the multimodal joint information, and solid ellipses indicate the task-relevant region.

B. Conceptual Explanation of Distributional Semantic Coherence

We provide a conceptual explanation of Distributional Semantic Coherence (DSC), as formally defined in Definition 3.4. The central idea of DSC is that multimodal semantic alignment should be understood at the level of latent semantic concepts, rather than through sample-wise or instance-level correspondence.

Multimodal data are inherently heterogeneous, and the information observed by different modalities often overlaps only partially and asymmetrically. Moreover, the set of semantic concepts shared across modalities can vary over time and context. For instance, in a video containing both a drum and a person, some segments may involve the drum being played (visual: drum and person, audio: drum sound), while others may involve the person speaking (visual: drum and person, audio: human voice). In such cases, the semantic correspondence between modalities shifts across segments, making rigid instance-level alignment assumptions inadequate. As a result, enforcing sample-level hard alignment, such as directly matching drum sounds to drum+person instances, fails to adequately capture the contextual and asymmetric nature of multimodal semantics.

To address this challenge, our model processes each modality using a Mixture-of-Experts (MoE) architecture, where each expert is encouraged to specialize in a distinct latent semantic concept. Inputs are routed probabilistically rather than deterministically, allowing each feature to contribute to multiple concepts. Importantly, features from different modalities that correspond to the same semantic concept can co-activate the same expert or a consistent subset of experts. This design enables semantic concepts to serve as shared intermediates across modalities, rather than enforcing direct alignment between raw modality-specific features.

Under this formulation, cross-modal alignment does not arise from enforcing direct correspondence between individual samples. Instead, alignment emerges through repeated co-activation of concept-specific experts associated with the same semantic concept across modalities. In some samples, a drum-related expert may be jointly activated by both audio and visual inputs, while in others, a person-related expert may dominate the alignment signal. Across diverse contexts and combinations of multimodal inputs, each semantic concept is repeatedly routed through the same expert(s) and updated via cross-modal contrastive learning. Through this process, semantic alignment is accumulated at the level of the data distribution, rather than being imposed at the level of individual samples.

The term distributional emphasizes that semantic coherence is established through statistical regularities observed across the dataset, not through explicit, one-to-one alignments within single samples. Each semantic concept appears in diverse contexts and alongside varying co-occurring entities. By consistently activating the same expert(s) across such variations, the model learns modality-invariant representations that remain robust to contextual changes. We refer to this property as Distributional Semantic Coherence, reflecting a form of multimodal alignment that respects the heterogeneous and context-dependent nature of real-world multimodal data.

C. Related Works

C.1. Multimodal Representation Learning

Multimodal representation learning (MMRL) aims to integrate information from heterogeneous modalities into semantically coherent representations. A dominant paradigm in this field is multimodal contrastive learning, which aligns representations from different modalities within a shared embedding space (Khan et al., 2025; Choi et al., 2025; Jiang et al., 2023; Park et al., 2024). CLIP-style models exemplify this approach, achieving strong performance across diverse downstream tasks (Radford et al., 2021; Li et al., 2021; 2022; Cherti et al., 2023). However, in realistic scenarios where modalities exhibit partial overlap or asymmetry, contrastive objectives can become sensitive to modality-specific signals, leading to unstable or distorted alignments (Jiang et al., 2023; Liang et al., 2022; Schrodri et al., 2025; Liao et al., 2025). To address this, several studies introduce regularization to suppress unique modality information (Almudévar et al., 2025). However, such shared-information centric alignment may discard task-relevant signals when downstream tasks rely on modality-unique cues, a limitation that has been both theoretically and empirically observed (Liang et al., 2023; Wang et al., 2025).

An alternative line of research adopts InfoMax-based objectives, aiming to preserve as much information as possible within each modality (Jiang et al., 2023; Dong et al., 2023). These approaches typically employ latent factorization or disentangled representation structures to explicitly model both shared and modality-unique components. For instance, Wang et al. (2025) propose DisentangledSSL, which sequentially learns shared and modality-unique representations using an information-theoretic criterion. Similarly, Liu et al. (2023) introduce a contrastive framework that orthogonally decomposes multimodal time-series data into shared and unique latent features, while jointly enforcing modality consistency, transformation consistency, and temporal locality. Related ideas have also been explored in domains such as single-cell multimodal analysis and T-cell receptor design (Zhang et al., 2024a; Li et al., 2023).

Nevertheless, InfoMax-oriented approaches tend to preserve task-irrelevant variability alongside useful information, which can adversely affect downstream performance (Poole et al., 2020; Soatto & Chiuso, 2016). To address this issue, Liang et al. (2023) propose an objective based on multi-view redundancy (Tian et al., 2020; Bachman et al., 2019; Hjelm et al., 2019), estimating task-relevant information through multimodal augmentation. By enforcing invariance across augmented views and leveraging bounds on mutual information, their method aims to suppress unnecessary variability. However, this approach relies on the assumption that task-relevant factors remain invariant under the chosen augmentations, making performance sensitive to augmentation quality and design.

In contrast to refining objectives alone, this work focuses on the structural organization of multimodal representations. We consider representations that decompose inputs into semantically interpretable components and allow selective recombination based on downstream task requirements. Such structural flexibility enables a more fine-grained correspondence between information and task demands, providing a complementary perspective to existing MMRL paradigms.

C.2. Mixture-of-Experts Models

Mixture-of-Experts (MoE) models employ conditional computation by selectively activating a subset of experts based on the input, allowing for efficient scaling of model capacity without a proportional increase in computation (Shazeer et al., 2017; Lepikhin et al., 2021). This design has been adopted in Transformer-based architectures to support large-scale training under limited resources (Rajbhandari et al., 2022; Fedus et al., 2022; Du et al., 2022). In these models, experts are treated as computational units, and routing is primarily used to distribute computational load and maintain training stability. Consequently, expert selection is driven more by efficiency considerations than by semantic structuring of representations.

Multimodal Mixture-of-Experts. To address the increasing computational demands and scalability challenges in multimodal settings, recent works have adapted MoE architectures to support multimodal inputs. For example, Mustafa et al. (2022), Shen et al. (2023), and Li et al. (2025) apply sparse MoE to image-text and omnimodal models, activating only a subset of experts to enhance efficiency and scalability. These works largely build upon conventional MoE research, adapting it for large-scale multimodal model training. Beyond scaling, some approaches utilize MoE to enhance robustness under missing modality scenarios. Yun et al. (2024) and Han et al. (2024) propose routing mechanisms that dynamically select experts based on observed modalities or infer missing information. Other studies apply multimodal MoE architectures to domain-specific tasks such as continual learning (Huai et al., 2025) and recommender systems (Bian et al., 2023).

While these methods focus on scaling, robustness, or domain adaptation, they typically lack explicit mechanisms for controlling the semantic structure of learned representations. Routing is primarily optimized for computational or adaptive

efficiency, with limited emphasis on selectively preserving, suppressing, or structurally disentangling information based on task-specific semantics.

MoE for Interpretability and Semantic Decomposition. More recently, a new line of research explores MoE not merely as a tool for efficiency, but as a structural prior for semantic decomposition and model interpretability. These studies reinterpret experts as semantically meaningful units, rather than as purely computational blocks. For instance, [Park et al. \(2025\)](#) decomposes the feedforward layers of large language models into 262K monosemantic experts, each specialized for distinct semantic features. This approach mitigates the polysemantic neuron problem and enables fine-grained analysis of model activations, demonstrating both mechanistic interpretability and functional manipulability. Similarly, [Yang et al. \(2025\)](#) promotes expert-level semantic specialization by combining sparsity-aware routing with ReLU-induced activation sparsity. [Oldfield et al. \(2025\)](#) critiques neuron-level sparse autoencoder approaches ([Huben et al., 2024](#); [Bricken et al., 2023](#)) for their performance degradation, and proposes the Mixture of Decoders, which introduces layer-level instead.

While these approaches highlight the inductive potential of MoE for structured representation, their focus remains on analyzing model internals or enhancing interpretability. In contrast, they do not offer explicit mechanisms for regulating which semantic information should be retained or discarded based on downstream task requirements, nor do they address task-driven selection and pruning from an information-theoretic standpoint.

Multitask Mixture-of-Experts. MoE has also been widely adopted in multitask learning to mitigate task interference and enable flexible parameter sharing ([Chen et al., 2023](#); [liang et al., 2022](#)). For example, [Ma et al. \(2018\)](#) propose a multi-gate MoE to address performance degradation in shared-bottom models when task relatedness is low, allowing each task to dynamically select its own expert composition. [liang et al. \(2022\)](#) dynamically adjust the number of active experts based on task difficulty to reduce gradient conflicts. Other works explore task-specific expert routing via memory-based selection ([Ye & Xu, 2023](#)) or domain-aware routing in multi-domain multitask settings ([Zhang et al., 2024b](#)). These models are trained end-to-end with supervised losses, where routing serves to separate tasks and reduce interference, rather than to explicitly regulate the semantic content of representations.

In contrast, our approach leverages MoE as a structural prior for semantic decomposition. During self-supervised pretraining, experts are encouraged to specialize according to latent semantic factors. At fine-tuning, we freeze both the backbone and experts, adapting only the router to selectively activate task-relevant experts. Unlike conventional multitask MoE approaches, where routing is optimized solely for predictive accuracy, our router functions as an information-theoretic bottleneck: it is trained to control the semantic flow, preserving only task-sufficient information while discarding irrelevant components.

D. Proofs of Problem Formulation

D.1. Proof of Proposition 2.1 (Data Processing Inequality)

For convenience, we denote $X = (X^1, X^2)$ and $Z = (Z^1, Z^2)$. Under the Markov chain assumption $Y \rightarrow X \rightarrow Z$ in Equation (1), the joint distribution factorizes as $p(y, x, z) = p(y)p(x|y)p(z|x)$, which implies that Y and Z are conditionally independent given X :

$$p(y, z|x) = p(y|x)p(z|x) \iff I(Z; Y|X) = 0. \tag{34}$$

We now apply the chain rule of mutual information:

$$I(X; Y) = I(Z, X; Y) - I(Z; Y|X) \tag{35}$$

$$= I(Z, X; Y) \quad (\because I(Z; Y|X) = 0, \text{ Equation (34)}) \tag{36}$$

$$= I(Z; Y) + I(X; Y|Z) \quad (\text{by chain rule: } I(Z, X; Y) = I(Z; Y) + I(X; Y|Z)) \tag{37}$$

$$\geq I(Z; Y). \quad (\because \text{non-negativity of conditional MI}) \tag{38}$$

The equality holds if and only if $I(X; Y|Z) = 0$, which means that Z is a sufficient statistic for Y with respect to X . In this case, (Z^1, Z^2) retains all task-relevant information in (X^1, X^2) for predicting Y . \square

D.2. Proof of Proposition 2.3 (Mutual Information Decomposition)

According to Definition 2.2, we decompose the input modalities as $X^1 = (X_S, X_U^1)$ and $X^2 = (X_S, X_U^2)$. Applying the chain rule of mutual information, we have:

$$I(X^1; X^2) = I(X_S, X_U^1; X_S, X_U^2) \quad (39)$$

$$= I(X_S; X_S, X_U^2) + I(X_U^1; X_S, X_U^2 | X_S) \quad (40)$$

$$= [I(X_S; X_S) + I(X_S; X_U^2 | X_S)] + [I(X_U^1; X_U^2 | X_S) + I(X_U^1; X_S | X_S, X_U^2)] \quad (41)$$

$$= I(X_S; X_S) + 0 + 0 + 0 \quad (\because X_S \perp X_U^1, X_S \perp X_U^2, X_U^1 \perp X_U^2) \quad (42)$$

$$= H(X_S). \quad (43)$$

Therefore, the modality-unique factors X_U^1 and X_U^2 do not contribute to the mutual information between X^1 and X^2 , which is solely determined by the shared factor X_S . \square

D.3. Proof of Proposition 2.5 (Fundamental Limitation of Contrastive Representations)

Proposition 2.3 shows that the cross-modal mutual information $I(X^1; X^2)$ is entirely determined by the shared factor X_S . This implies that multimodal contrastive learning, by design, optimizes only for aligning shared information across modalities, without any pressure to preserve modality-unique factors (X_U^1, X_U^2) . As a result, the optimal solution induced by contrastive objectives corresponds to a shared-only representation that satisfies:

$$(X_U^1, X_U^2) \perp (Z_{CL}^1, Z_{CL}^2) | X_S. \quad (44)$$

Now consider a downstream task that relies on the unique factors. According to Definition 2.4, this implies:

$$I(X_U^1, X_U^2; Y) > 0. \quad (45)$$

In other words, the presence of nonzero mutual information $I(X_U^1, X_U^2; Y)$ indicates that X_S alone is insufficient for predicting Y , as the unique factors X_U^1 and X_U^2 carry task-relevant information.

$$I(X^1, X^2; Y | Z_{CL}^1, Z_{CL}^2) = I(X_S, X_U^1, X_U^2; Y | Z_{CL}^1, Z_{CL}^2) \quad (46)$$

$$\geq I(X_U^1, X_U^2; Y | Z_{CL}^1, Z_{CL}^2) \quad (47)$$

$$\geq I(X_U^1, X_U^2; Y | X_S) \quad (\because \text{Markov chain Equation (7)}) \quad (48)$$

$$= I(X_U^1, X_U^2; Y) \quad (\because X_S \perp X_U^1, X_S \perp X_U^2) \quad (49)$$

$$> 0. \quad (50)$$

According to Section D.1, if $I(X^1, X^2; Y | Z_{CL}^1, Z_{CL}^2) > 0$, then the representation (Z_{CL}^1, Z_{CL}^2) cannot be a sufficient statistic for Y . In this case, the strict inequality form of the data processing inequality (DPI) holds:

$$I(X^1, X^2; Y) > I(Z_{CL}^1, Z_{CL}^2; Y). \quad (51)$$

\square

E. Estimating Mutual Information Objectives

E.1. InfoNCE as a Lower Bound on Mutual Information

The InfoNCE (Noise-Contrastive Estimation) loss is widely used as a variational lower bound estimator of mutual information $I(X; Z)$. The derivation presented here follows the standard formulation from van den Oord et al. (2018). The mutual information is defined as:

$$I(X; Z) = \mathbb{E}_{p(x,z)} \left[\log \frac{p(x|z)}{p(x)} \right]. \quad (52)$$

In practice, the true densities $p(x)$ and $p(x|z)$ are not accessible, so we introduce a non-negative score function $\psi(x, z)$ to approximate the log-density ratio $\log \frac{p(x|z)}{p(x)}$. A common instantiation defines $\psi(x, z) := \langle f(x), z \rangle / \tau$, where $f(x)$ is an

encoder, $\langle \cdot, \cdot \rangle$ denotes cosine similarity between ℓ_2 -normalized vectors, and τ is a temperature hyperparameter. Assuming that $\psi(x, z)$ approximates the log-density ratio, we obtain:

$$\exp(\psi(x, z)) \propto \frac{p(x|z)}{p(x)}. \quad (53)$$

Given a batch $\mathcal{B} = \{1, \dots, B\}$, the InfoNCE loss for a positive pair (x_i, z_i) is defined in the form of a cross-entropy:

$$\mathcal{L}_{\text{InfoNCE}} = -\mathbb{E}_i \left[\log \frac{\exp(\psi(x_i, z_i))}{\sum_j \exp(\psi(x_i, z_j))} \right]. \quad (54)$$

Substituting the density ratio approximation into Equation (54), we have:

$$\mathcal{L}_{\text{InfoNCE}} = -\mathbb{E}_i \left[\log \frac{\frac{p(x_i|z_i)}{p(x_i)}}{\frac{p(x_i|z_i)}{p(x_i)} + \sum_{j \neq i} \frac{p(x_i|z_j)}{p(x_i)}} \right] \quad (55)$$

$$= \mathbb{E}_i \left[\log \left(1 + \frac{p(x_i)}{p(x_i|z_i)} \sum_{j \neq i} \frac{p(x_i|z_j)}{p(x_i)} \right) \right] \quad (56)$$

$$\approx \mathbb{E}_i \left[\log \left(1 + \frac{p(x_i)}{p(x_i|z_i)} (B-1) \mathbb{E}_j \left[\frac{p(x_i|z_j)}{p(x_i)} \right] \right) \right] \quad (57)$$

$$= \mathbb{E}_i \left[\log \left(1 + \frac{p(x_i)}{p(x_i|z_i)} (B-1) \right) \right] \quad (58)$$

$$\geq \mathbb{E}_i \left[\log \left(\frac{p(x_i)}{p(x_i|z_i)} B \right) \right] \quad (59)$$

$$= -I(X; Z) + \log B. \quad (60)$$

Here, we make a standard assumption that the negative samples z_j (for $j \neq i$) are drawn independently of the anchor x_i , implying $p(x_i|z_j) \approx p(x_i)$. Therefore, InfoNCE provides the following variational lower bound on mutual information:

$$I(X; Z) \geq \log B - \mathcal{L}_{\text{InfoNCE}}. \quad (61)$$

Minimizing $\mathcal{L}_{\text{InfoNCE}}$ is thus equivalent to maximizing this lower bound, encouraging the encoder to preserve as much information about X in Z as possible. \square

E.2. SupCon as a Lower Bound on Task-Conditioned Mutual Information

In this section, we show that the supervised contrastive (SupCon) loss (Khosla et al., 2020) serves as a variational lower bound estimator of the mutual information $I(Z; Y)$ between the learned representation Z and the label Y . The target mutual information is defined as:

$$I(Z; Y) = \mathbb{E}_i \left[\log \frac{p(z_i|y_i)}{p(z_i)} \right]. \quad (62)$$

Given a batch $\mathcal{B} = \{1, \dots, B\}$ and a set of positive indices $\mathcal{S}_{y_i} = \{s \mid y_s = y_i\}$ that share the same label as anchor i , the SupCon loss is defined as:

$$\mathcal{L}_{\text{SupCon}} = -\mathbb{E}_i \mathbb{E}_s \left[\log \frac{\exp(\psi(z_i, z_s))}{\sum_j \exp(\psi(z_i, z_j))} \right]. \quad (63)$$

where the score function is defined as $\psi(z_i, z_j) := \langle z_i, z_j \rangle / \tau$, using cosine similarity between ℓ_2 -normalized representations and a temperature parameter τ . The index s is uniformly sampled from the empirical positive set \mathcal{S}_{y_i} , and we write \mathbb{E}_s to denote expectation over this set. Since the log function is concave, we apply Jensen's inequality to obtain a lower bound on

the inner expectation:

$$\mathbb{E}_s \left[\log \frac{\exp(\psi(z_i, z_s))}{\sum_j^B \exp(\psi(z_i, z_j))} \right] \leq \log \left(\mathbb{E}_s \left[\frac{\exp(\psi(z_i, z_s))}{\sum_j^B \exp(\psi(z_i, z_j))} \right] \right) \quad (64)$$

$$= \log \left(\frac{1}{|\mathcal{S}_{y_i}|} \sum_{s \in \mathcal{S}_{y_i}} \frac{\exp(\psi(z_i, z_s))}{\sum_j^B \exp(\psi(z_i, z_j))} \right) \quad (65)$$

$$= \log \left(\frac{\frac{1}{|\mathcal{S}_{y_i}|} \sum_{s \in \mathcal{S}_{y_i}} \exp(\psi(z_i, z_s))}{\sum_j^B \exp(\psi(z_i, z_j))} \right). \quad (66)$$

Substituting this back into the definition of SupCon in Equation (63), we obtain the following lower bound:

$$\mathcal{L}_{\text{SupCon}} \geq -\mathbb{E}_i \left[\log \left(\frac{\frac{1}{|\mathcal{S}_{y_i}|} \sum_{s \in \mathcal{S}_{y_i}} \exp(\psi(z_i, z_s))}{\sum_j^B \exp(\psi(z_i, z_j))} \right) \right] \quad (67)$$

We now reinterpret the exponential score $\exp(\psi(z_i, z))$ as a non-parametric kernel function in a kernel density estimation (KDE) framework, similar to the analysis in Section E.1. Under this view, the numerator in Equation (67) corresponds to a batch-wise KDE estimator of the class-conditional density $p(z_i|y_i)$, constructed from the empirical positive set \mathcal{S}_{y_i} . The denominator serves as a KDE estimator of the marginal density $p(z_i)$ over the full batch. Accordingly, we define the estimators as:

$$\hat{p}(z_i|y_i) = \frac{1}{|\mathcal{S}_{y_i}|} \sum_{s \in \mathcal{S}_{y_i}} \exp(\psi(z_i, z_s)), \quad \hat{p}(z_i) = \frac{1}{B} \sum_j^B \exp(\psi(z_i, z_j)). \quad (68)$$

Substituting these estimators into Equation (67) yields:

$$\mathcal{L}_{\text{SupCon}} \geq -\mathbb{E}_i \left[\log \left(\frac{\frac{1}{|\mathcal{S}_{y_i}|} \sum_{s \in \mathcal{S}_{y_i}} \exp(\psi(z_i, z_s))}{B \cdot \frac{1}{B} \sum_j^B \exp(\psi(z_i, z_j))} \right) \right] \quad (69)$$

$$= -\mathbb{E}_i \left[\log \left(\frac{\hat{p}(z_i|y_i)}{B \cdot \hat{p}(z_i)} \right) \right] \quad (70)$$

$$= -\mathbb{E}_i \left[\log \frac{\hat{p}(z_i|y_i)}{\hat{p}(z_i)} - \log B \right] \quad (71)$$

$$= -\mathbb{E}_i \left[\log \frac{\hat{p}(z_i|y_i)}{\hat{p}(z_i)} \right] + \log B \quad (72)$$

$$\approx -\mathbb{E}_i \left[\log \frac{p(z_i|y_i)}{p(z_i)} \right] + \log B \quad (73)$$

$$= -I(Z; Y) + \log B. \quad (74)$$

Therefore, SupCon yields the following variational lower bound on the task-conditioned mutual information:

$$I(Z; Y) \geq \log B - \mathcal{L}_{\text{SupCon}}. \quad (75)$$

□

E.3. KL Divergence to vMF for Compactness-Based Information-Minimality

To quantify the extent to which the learned representation Z retains task-irrelevant information from the input X given the downstream target Y , we consider the conditional mutual information $I(Z; X|Y)$. Under the Markov assumption

$Y \rightarrow X \rightarrow Z$ (Equation (1)), this can be reformulated as follows:

$$I(Z; X|Y) = \mathbb{E}_{p(z,x,y)} \left[\log \frac{p(z, x|y)}{p(z|y)p(x|y)} \right] \quad (76)$$

$$= \mathbb{E}_{p(z,x,y)} \left[\log \frac{p(z|x, y)p(x|y)}{p(z|y)p(x|y)} \right] \quad (77)$$

$$= \mathbb{E}_{p(z,x,y)} \left[\log \left(\frac{p(z|x)}{p(z|y)} \right) \right] \quad (\because Y \rightarrow X \rightarrow Z) \quad (78)$$

$$= \mathbb{E}_{p(x,y)} \left[\mathbb{E}_{p(z|x)} \left[\log \left(\frac{p(z|x)}{p(z|y)} \right) \right] \right] \quad (79)$$

$$= \mathbb{E}_{p(x,y)} [D_{\text{KL}}(p(z|x) \parallel p(z|y))]. \quad (80)$$

Thus, minimizing $I(Z; X|Y)$ reduces to minimizing the KL divergence between the conditional distributions $p(z|x)$ and $p(z|y)$. However, directly computing this KL divergence is intractable due to the unknown forms of the underlying distributions. To address this, we approximate both $p(z|x)$ and $p(z|y)$ using von Mises–Fisher (vMF) distributions, motivated by the fact that the representations $f(x)$ are ℓ_2 -normalized and lie on the unit hypersphere after pretraining via InfoNCE in the specialization stage. The vMF distribution over a unit vector $z \in \mathbb{R}^d$ is defined as:

$$\text{vMF}(z; \mu, \kappa) = C_d(\kappa) \exp(\kappa \mu^\top z). \quad (81)$$

where μ is a unit vector denoting the mean direction, κ is the concentration parameter, and $C_d(\kappa)$ is the normalization constant. We approximate the conditional distributions using vMF distributions. Specifically, the instance-level distribution $p(z|x)$ is modeled as a vMF distribution centered at the sample-specific mean direction $\mu_x = f(x)$, where f denotes the encoder mapping input x to its ℓ_2 -normalized representation. In contrast, the class-level distribution $p(z|y)$ is approximated by a vMF distribution whose mean direction $\hat{\mu}_y$ is obtained by normalizing the empirical class mean vector, defined as $\mu_y = \frac{1}{|\mathcal{S}_y|} \sum_{s \in \mathcal{S}_y} z_s$, where \mathcal{S}_y denotes the set of samples sharing the same class label y , as defined in Section E.2:

$$p(z|x) = \text{vMF}(z; \mu_x, \kappa_x), \quad p(z|y) = \text{vMF}(z; \hat{\mu}_y, \kappa_y). \quad (82)$$

The KL divergence between the two vMF distributions becomes:

$$D_{\text{KL}}(p(z|x) \parallel p(z|y)) = \mathbb{E}_{p(z|x)} \left[\log \frac{p(z|x)}{p(z|y)} \right] \quad (83)$$

$$= \mathbb{E}_{p(z|x)} \left[\log \frac{C_d(\kappa_x) \exp(\kappa_x \mu_x^\top z)}{C_d(\kappa_y) \exp(\kappa_y \hat{\mu}_y^\top z)} \right] \quad (84)$$

$$= \mathbb{E}_{p(z|x)} \left[\log \left(\frac{C_d(\kappa_x)}{C_d(\kappa_y)} \right) + \kappa_x \mu_x^\top z - \kappa_y \hat{\mu}_y^\top z \right] \quad (85)$$

$$= \log \left(\frac{C_d(\kappa_x)}{C_d(\kappa_y)} \right) + \kappa_x \mathbb{E}_{p(z|x)} [\mu_x^\top z] - \kappa_y \mathbb{E}_{p(z|x)} [\hat{\mu}_y^\top z]. \quad (86)$$

For a vMF distribution $\text{vMF}(z; \mu, \kappa)$, the expected value is $\mathbb{E}[z] = A_d(\kappa)\mu$, where $A_d(\kappa)$ denotes the mean resultant length of the vMF distribution. Therefore, we compute:

$$\mathbb{E}_{p(z|x)} [\mu_x^\top z] = \mu_x^\top \mathbb{E}_{p(z|x)} [z] = \mu_x^\top (A_d(\kappa_x)\mu_x) = A_d(\kappa_x) (\mu_x^\top \mu_x) = A_d(\kappa_x), \quad (87)$$

$$\mathbb{E}_{p(z|x)} [\hat{\mu}_y^\top z] = \hat{\mu}_y^\top \mathbb{E}_{p(z|x)} [z] = \hat{\mu}_y^\top (A_d(\kappa_x)\mu_x) = A_d(\kappa_x) (\mu_x^\top \hat{\mu}_y). \quad (88)$$

Plugging these in, we obtain the closed-form KL divergence:

$$D_{\text{KL}}(p(z|x) \parallel p(z|y)) = \log \left(\frac{C_d(\kappa_x)}{C_d(\kappa_y)} \right) + \kappa_x A_d(\kappa_x) - \kappa_y A_d(\kappa_x) (\mu_x^\top \hat{\mu}_y). \quad (89)$$

However, the above expression still involves $C_d(\kappa)$ and $A_d(\kappa)$, both of which are defined in terms of modified Bessel functions and are computationally expensive to evaluate. To make this expression more tractable, we follow the common

simplification of assuming identical concentration parameters: $\kappa_x = \kappa_y = \kappa$. This assumption corresponds to modeling equal intra-class and instance-level concentration. This yields:

$$D_{\text{KL}}(p(z|x) \parallel p(z|y)) = \log \left(\frac{C_d(\kappa)}{C_d(\kappa)} \right) + \kappa A_d(\kappa) - \kappa A_d(\kappa) (\mu_x^\top \hat{\mu}_y) \quad (90)$$

$$= \kappa A_d(\kappa) (1 - \mu_x^\top \hat{\mu}_y). \quad (91)$$

As a result, the conditional mutual information admits the following proportional surrogate:

$$\mathbb{E}_{p(x,y)} [D_{\text{KL}}(p(z|x) \parallel p(z|y))] \propto -\mathbb{E}_{p(x,y)} [\mu_x^\top \hat{\mu}_y]. \quad (92)$$

Hence, minimizing $I(Z; X|Y)$ can be achieved via a tractable surrogate that maximizes the cosine similarity between each sample’s direction vector and its class-conditional mean direction. \square

F. Auxiliary Losses

To ensure stable and meaningful expert utilization in the Mixture-of-Experts (MoE) architecture, we employ four auxiliary losses that guide the router g to assign tokens effectively and encourage specialization across experts. Since the MoE router adopts top- k sparse routing, it is prone to training instabilities such as expert collapse and assignment imbalance. These issues hinder effective use of model capacity and compromise expert-level diversity and specialization. To mitigate these challenges, we incorporate and adapt several strategies proposed in prior works (Shazeer et al., 2017; Riquelme et al., 2021; Mustafa et al., 2022) to fit our framework. Specifically, our auxiliary loss is defined as a weighted sum of four components:

$$\mathcal{L}_{\text{aux}} = \lambda_{\text{imp}} \mathcal{L}_{\text{imp}} + \lambda_{\text{load}} \mathcal{L}_{\text{load}} + \lambda_{\text{local}} \mathcal{L}_{\text{local}} + \lambda_{\text{global}} \mathcal{L}_{\text{global}}. \quad (93)$$

Each component is defined based on token-level routing statistics within a training batch. Let $\mathcal{B} = \{1, \dots, B\}$ denote the set of batch indices, and let the intermediate representation of each sample be given by a sequence $[\mathbf{x}_{b,t}]_{t=1}^{T_b}$, where $\mathbf{x}_{b,t} \in \mathbb{R}^{D_{\text{model}}}$. Here, T_b denotes the sequential length of the input sample b . We define the set of all tokens in the batch as $\mathbf{X} = \{\mathbf{x}_{b,t} \mid b \in \mathcal{B}, t = 1, \dots, T_b\}$.

F.1. Importance Loss

The importance loss encourages balanced utilization of experts by enforcing that the total soft routing weight assigned to each expert is approximately uniform across the batch. From a soft-routing perspective, this objective mitigates the tendency of routing probabilities to concentrate excessively on a small subset of experts. Formally, the importance of expert i is defined as

$$\text{Imp}_i(\mathbf{X}) = \sum_{\mathbf{x} \in \mathbf{X}} \text{softmax}(\mathbf{W}_g \mathbf{x})_i, \quad (94)$$

where \mathbf{W}_g denotes the linear projection associated with the router. If the resulting importance vector $\text{Imp}(\mathbf{X}) = \{\text{Imp}_i(\mathbf{X})\}_{i=1}^{N_{\text{expert}}}$ is highly imbalanced, routing weights may collapse onto a small number of experts, leading to degraded specialization and inefficient use of model capacity. To prevent this behavior, we penalize the dispersion of the importance distribution by minimizing its coefficient of variation:

$$\mathcal{L}_{\text{imp}} = \left(\frac{\text{std}(\text{Imp}(\mathbf{X}))}{\text{mean}(\text{Imp}(\mathbf{X}))} \right)^2 \propto \text{var}(\text{Imp}(\mathbf{X})). \quad (95)$$

F.2. Load Loss

While the importance loss promotes balanced soft routing weights, it does not guarantee balanced hard assignments due to the nature of top- k selection. In practice, even with a uniform importance distribution, the router may repeatedly assign tokens to a small subset of experts, leaving others unused. Load loss directly addresses this assignment imbalance by encouraging equalized expert selection. However, since the number of assigned tokens is a discrete and non-differentiable quantity, we adopt a probabilistic proxy following Shazeer et al. (2017); Riquelme et al. (2021). Specifically, we estimate the probability that expert i is selected in the top- k for a given token $\mathbf{x}_{b,t}$. During the forward pass, we add Gaussian noise

to the expert scores, yielding $\mathbf{W}_g \mathbf{x}_{b,t} + \epsilon$, where $\epsilon \sim \mathcal{N}(0, \sigma^2)$ and $\sigma = \frac{1}{N_{\text{expert}}}$ controls the noise scale. The top- k threshold is then defined as the k -th largest value among the noisy scores:

$$\text{threshold}_k(\mathbf{x}_{b,t}) = \max_{k\text{-th}}(\mathbf{W}_g \mathbf{x}_{b,t} + \epsilon). \quad (96)$$

To compute the selection probability of expert i , we re-sample an independent noise term $\epsilon_{\text{new}} \sim \mathcal{N}(0, \sigma^2)$ and estimate the probability that expert i 's score exceeds the top- k threshold:

$$p_i(\mathbf{x}) = P((\mathbf{W}_g \mathbf{x}_{b,t})_i + \epsilon_{\text{new}} \geq \text{threshold}_k(\mathbf{x}_{b,t})) \quad (97)$$

$$= P(\epsilon_{\text{new}} \geq \text{threshold}_k(\mathbf{x}_{b,t}) - (\mathbf{W}_g \mathbf{x}_{b,t})_i). \quad (98)$$

Using these probabilities, we define the expected load of expert i over the batch as:

$$\text{load}_i(\mathbf{X}) = \sum_{\mathbf{x} \in \mathbf{X}} p_i(\mathbf{x}), \quad (99)$$

$$\text{load}(\mathbf{X}) = \{\text{load}_i(\mathbf{X})\}_{i=1}^{N_{\text{expert}}}. \quad (100)$$

Finally, to encourage balanced load across experts, we minimize the squared coefficient of variation of the load distribution:

$$\mathcal{L}_{\text{load}} = \left(\frac{\text{std}(\text{load}(\mathbf{X}))}{\text{mean}(\text{load}(\mathbf{X}))} \right)^2 \propto \text{var}(\text{load}(\mathbf{X})). \quad (101)$$

F.3. Local Entropy Loss

In each MoE layer, the router produces a probabilistic distribution over experts for every input token. For a given token $\mathbf{x}_{b,t}$, the expert routing distribution is defined as

$$p(\text{expert} \mid \mathbf{x}_{b,t}) \in \mathbb{R}^{N_{\text{expert}}}, \quad (102)$$

which represents the relative contribution or routing strength of each expert in processing the token. The top- k operation subsequently selects a subset of experts based on this distribution. The local entropy loss is defined as the average entropy of the token-level routing distributions across the batch:

$$\mathcal{L}_{\text{local}} = \mathbb{E}_{\mathbf{x} \in \mathbf{X}} [H(p(\text{expert} \mid \mathbf{x}))], \quad (103)$$

where $H(\cdot)$ denotes the standard Shannon entropy. Minimizing $\mathcal{L}_{\text{local}}$ encourages lower entropy in the routing distributions, thereby promoting more confident and concentrated assignments of each token to a small number of experts. This sharpening of token-level routing encourages consistent and decisive expert selection, which in turn strengthens expert-level specialization by reducing overlap among expert responsibilities.

F.4. Global Entropy Loss

While the local entropy loss encourages sharp and confident expert selection at the token level, the global entropy loss promotes diversity in expert utilization from a batch-level perspective. To quantify the overall distribution of expert usage, we compute the average routing distribution across all tokens in the batch:

$$\tilde{p}(\text{experts}) = \mathbb{E}_{\mathbf{x} \in \mathbf{X}} [p(\text{expert} \mid \mathbf{x}_{b,t})] \in \mathbb{R}^{N_{\text{expert}}}, \quad (104)$$

where $\tilde{p}(\text{experts})$ represents the marginal expert utilization across the batch. It reflects the average routing weight received by each expert. If this distribution is highly skewed toward a few experts, it may lead to expert collapse and underutilization of model capacity. To mitigate this issue, the global entropy loss encourages the marginal distribution to approach uniformity by maximizing its entropy. Specifically, it is defined as:

$$\mathcal{L}_{\text{global}} = -H(\tilde{p}_m(\text{experts})). \quad (105)$$

G. Experimental Details

G.1. Dataset Description

We conduct experiments on four representative benchmarks provided by the real-world multimodal benchmark suite, MultiBench (Liang et al., 2021). MultiBench covers a wide range of multimodal tasks across domains and provides pre-extracted modality-specific features along with standardized evaluation protocols. Following prior works (Liang et al., 2023; Wang et al., 2025), we adopt the same input features and evaluation settings for fair comparison. The benchmarks used in our experiments are as follows:

1. MOSEI (Bagher Zadeh et al., 2018): A sentiment and emotion recognition benchmark comprising approximately 23,000 monologue video segments. Each sample is labeled with a sentiment intensity score in the range of $[-3, 3]$. Following Liang et al. (2023) and Wang et al. (2025), we convert the scores into binary labels (positive/negative) and use the provided vision and text features.
2. MOSI (Zadeh et al., 2016): A sentiment analysis benchmark similar to MOSEI, consisting of 2,199 short video clips from YouTube. Sentiment scores are similarly binarized, and vision and text features are used.
3. UR-FUNNY (Hasan et al., 2019): A humor detection benchmark built from TED Talk segments, containing over 16,000 samples. Each sample is labeled for the presence or absence of humor, using vision and text modalities.
4. MUSTARD (Castro et al., 2019): A sarcasm detection benchmark consisting of 690 video clips from TV shows such as Friends, The Golden Girls, and The Big Bang Theory. The task is framed as binary classification using pre-extracted vision and text features.

We exclude the MIMIC-III (Johnson et al., 2016) benchmark from our experiments. This dataset comprises time-series signals and tabular metadata from over 40,000 ICU patients. Prior works adopt GRUs for the time-series modality and MLPs for the tabular modality. In contrast, our method employs Transformer-based Mixture-of-Experts encoders across all modalities. Due to this architectural mismatch and the data structure of MIMIC-III, we exclude it from evaluation.

G.2. Implementation Details

We design our experiments to follow the settings of prior works (Liang et al., 2023; Wang et al., 2025) for fair comparison. For all benchmarks, we use the same data splits provided by MultiBench. Each modality is processed by an independent Mixture-of-Experts encoder, and the modality-specific feature encoders consist of 5 layers, following prior work. The expansion ratio ρ is fixed to 8 across all datasets, while the granularity χ and preservation ratio p are varied across experiments. All models are trained end-to-end from random initialization. After representation learning, performance is evaluated using linear probing by training a separate linear classifier. Following Wang et al. (2025), we report the mean and standard deviation of downstream prediction accuracy over three random seeds.

H. Additional Experimental Results

H.1. Entropy-Based Monitoring of Router Behavior at Selection Stage

During the Selection stage, the router is optimized to satisfy Task-Sufficiency and Information-Minimality by maximizing mutual information among label-consistent samples. While the attention and expert modules are frozen, only the lightweight router is fine-tuned. Although auxiliary losses are not used as training objectives in this stage, we monitor them throughout training to qualitatively analyze the behavior of the router. Specifically, we track both the local entropy loss (measuring per-token expert selection confidence) and the global entropy loss (measuring expert usage diversity across the batch), as defined in Section F. Figures 7 to 10 show the dynamics of local and global entropy for both modalities (vision and text) across different granularity settings ($\chi = 2, 4, 8$) for each dataset.

We observe that higher granularity leads to a decrease in local entropy, indicating more confident and deterministic expert selection over time. In contrast, at low granularity ($\chi = 2$), local entropy tends to decrease more slowly, fluctuate, or even increase, suggesting routing ambiguity and less reliable expert discrimination. These trends support our analysis in Section 6.1: at low granularity, each expert captures a broad mixture of semantic concepts due to the small number of large experts, resulting in greater semantic entanglement. This makes it more difficult for the router to identify task-relevant experts.

Furthermore, we observe that entropy stability is strongly influenced by dataset scale. Larger datasets such as MOSEI and UR-FUNNY exhibit lower per-step fluctuation. In contrast, smaller datasets such as MOSI and MUSTARD show greater per-step variance, indicating higher instability in expert selection during training. This observation aligns with the variance patterns discussed in Section 6.3, where smaller datasets were shown to induce higher performance variability due to limited data. The entropy-based monitoring thus provides further evidence that dataset scale impacts not only downstream accuracy but also the stability of the router’s expert selection process.

Finally, we note a consistent decrease in global entropy (i.e., increase in negative entropy) during training, reflecting the router’s tendency to converge toward a more selective usage of task-relevant experts. This outcome aligns with the label-consistency assumption underlying our Selection stage: samples with the same label are expected to activate semantically aligned experts, leading to sharper and more focused routing distributions.

H.2. Ablation Study

Selection Stage: Loss Combination Ablation. We analyze the individual and combined contributions of the two objectives used in the Selection stage: the Task-Sufficiency loss ($\mathcal{L}_{\text{suff}}$) and the Information-Minimality loss (\mathcal{L}_{min}). Table 3 reports results under the granularity setting $\chi = 8$, where only the router is fine-tuned on top of a model pretrained with the Specialization stage, using different combinations of the two losses.

$\mathcal{L}_{\text{suff}}$	\mathcal{L}_{min}	MOSEI	MOSI	UR-FUNNY	MUSTARD
		75.78(0.32)	63.56(2.18)	63.61(0.49)	58.70(3.16)
✓	✓	77.36(0.29)	64.29(1.27)	63.52(0.62)	61.59(0.72)
✓		77.53(0.50)	65.31(0.76)	64.08(0.57)	61.11(5.44)
	✓	77.07(0.31)	66.67(1.31)	64.18(0.74)	60.63(3.42)

Table 3. Ablation of router fine-tuning losses ($\chi = 8$). Prediction accuracy (%) on four benchmarks, averaged over three seeds (std. in parentheses). The first row corresponds to Specialization only, the others apply Selection with different loss combinations.

The first row corresponds to applying Specialization only, without the Selection stage, and yields consistently lower performance across all benchmarks. This indicates that, despite the structural expressiveness of the pretrained latent space, task-specific performance remains limited without explicit task-adaptive selection. The remaining rows show results obtained by fine-tuning the router using $\mathcal{L}_{\text{suff}}$ only, \mathcal{L}_{min} only, and their combination, respectively. In all datasets, applying the Selection stage leads to consistent performance improvements over the Specialization-only baseline.

Notably, although the two losses operate through different mechanisms, they result in comparable performance gains. The Task-Sufficiency loss ($\mathcal{L}_{\text{suff}}$) emphasizes task-relevant experts by promoting information sharing among label-consistent samples, while the Information-Minimality loss (\mathcal{L}_{min}) suppresses task-irrelevant experts by discouraging label-invariant variations. Despite these differing formulations, both objectives ultimately serve a common goal: highlighting task-relevant semantic components. The fact that each loss independently yields meaningful improvements supports the effectiveness of our design in inducing task-adaptive expert selection from complementary perspectives.

Applying Sparsification without the Selection Stage. We further examine the effect of applying Sparsification without the Selection stage, i.e., performing pruning directly after Specialization. Figure 6 visualizes the resulting pruning curves, using the same y-axis ranges and resolution as Figure 5 for direct comparison with the full S3 framework.

Overall, when Sparsification is applied without prior Selection, performance changes do not exhibit consistent or monotonic trends. This behavior arises because the router operates independently of task in this setting. Without explicitly identifying and emphasizing task-relevant experts, pruning cannot reliably distinguish between semantically important and unimportant routing paths, leading to structurally unpredictable performance variations.

These observations indicate that Sparsification is not an independent performance-improvement mechanism, but rather relies on the task-adaptive routing structure established during the Selection stage. Meaningful performance-efficiency trade-offs emerge only after task-relevant expert activations have been aligned. When applied in isolation, Sparsification fails to fully realize its structural benefits.

In summary, this ablation study demonstrates that the three stages of the S3 framework are not independently interchangeable. Instead, stable and interpretable task-adaptive sparsity emerges from their sequential structure: Specialization, Selection, Sparsification. Each stage provides the structural foundation for the next, and Sparsification becomes effective only after expert routing has been aligned with task semantics through the Selection stage.

Toward Structural Multimodal Representations: Specialization, Selection, and Sparsification via Mixture-of-Experts

DATASET	χ	0.9	0.8	0.7	0.6	0.5	0.4	0.3	0.2	0.1
MOSEI	2	96.61	93.23	89.84	86.45	83.07	79.68	76.30	72.91	69.52
	4	96.61	93.21	89.82	86.43	83.04	79.64	76.25	72.86	69.46
	8	96.59	93.19	89.78	86.38	82.97	79.57	76.16	72.75	69.35
MOSI	2	96.61	93.22	89.83	86.44	83.05	79.66	76.27	72.88	69.49
	4	96.60	93.21	89.81	86.41	83.02	79.62	76.22	72.82	69.43
	8	96.59	93.18	89.77	86.36	82.95	79.54	76.13	72.72	69.31
UR-FUNNY	2	96.70	93.41	90.11	86.82	83.52	80.23	76.93	73.64	70.34
	4	96.70	93.40	90.10	86.79	83.49	80.19	76.89	73.59	70.29
	8	96.69	93.37	90.06	86.74	83.43	80.11	76.80	73.48	70.17
MUSTARD	2	96.87	93.74	90.60	87.47	84.34	81.21	78.08	74.94	71.81
	4	96.86	93.71	90.57	87.42	84.28	81.13	77.99	74.85	71.70
	8	96.83	93.66	90.49	87.32	84.15	80.99	77.82	74.65	71.48

Table 5. Expected per-token parameter activate (%) across preservation ratios $p \in [0, 1]$ during the Sparsification stage. Values are normalized to 100% at $p = 1$. The metric reflects the average fraction of active parameters. The metric reflects the average fraction of active parameters involved in semantic transformation, attention, and expert computation, excluding the router.

H.3. Trainable Parameter Ratio in Selection Stage

To quantify the lightweight nature of the Selection stage, we report the ratio of trainable parameters involved in router fine-tuning. During this stage, all attention and expert layers are frozen, and only the router parameters are updated. Table 4 presents the proportion of trainable parameters relative to the total model size for each granularity setting ($\chi = 2, 4, 8$). As shown in the table, the router accounts for less than 1% of the total parameters in all cases, with values ranging from 0.0984% to 1.0708%. These results confirm that our Selection stage enables highly efficient fine-tuning with negligible parameter updates.

DATASET	χ		
	2	4	8
MOSEI	0.0984	0.2075	0.4574
MOSI	0.0984	0.2075	0.4574
UR-FUNNY	0.0982	0.2071	0.4565
MUSTARD	0.2059	0.4538	1.0708

Table 4. Ratio of trainable parameters during router fine-tuning in the Selection stage (%). We report the proportion of trainable parameters relative to the total model parameters for different granularity settings ($\chi = 2, 4, 8$). Only the router is updated, with attention and expert weights frozen.

H.4. Sparsification Efficiency Analysis

To analyze the computational efficiency of our sparsification stage, we measure the proportion of active parameters per token under varying preservation ratios. For each preservation ratio $p \in [0, 1]$, we compute the expected fraction of activated parameters per token, normalized to 100% at $p = 1$. As shown in Table 5, reducing the preservation ratio leads to a consistent decrease in active parameters across all datasets and granularities. These results validate the practicality of our sparsification stage as an inference-time efficiency control mechanism without requiring any additional training.

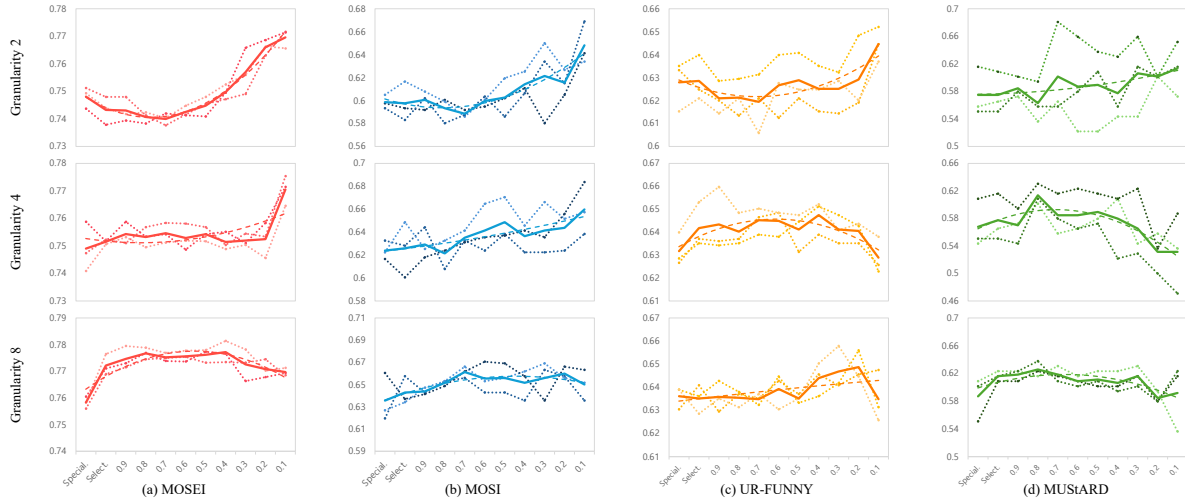


Figure 5. Performance across four benchmarks for $\chi \in \{2, 4, 8\}$. Solid lines show the mean over three random seeds, dashed lines their trend, and dotted lines individual seeds. All results follow the full S3 pipeline, with p progressively decreased during Sparsification.

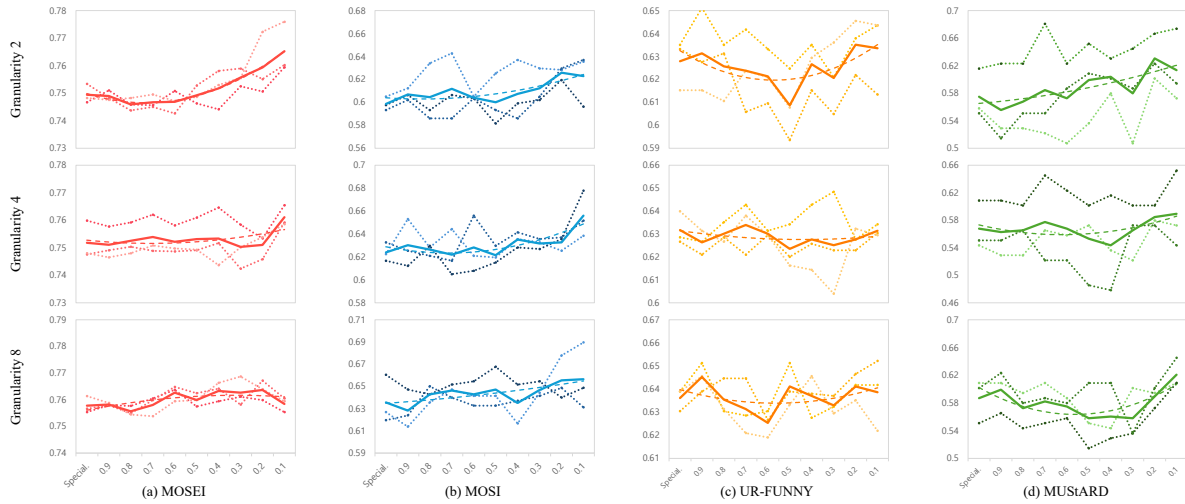


Figure 6. Performance when Sparsification is applied directly after Specialization, without the Selection stage. Results are shown for $\chi \in \{2, 4, 8\}$ using the same y-axis scale as Figure 5.

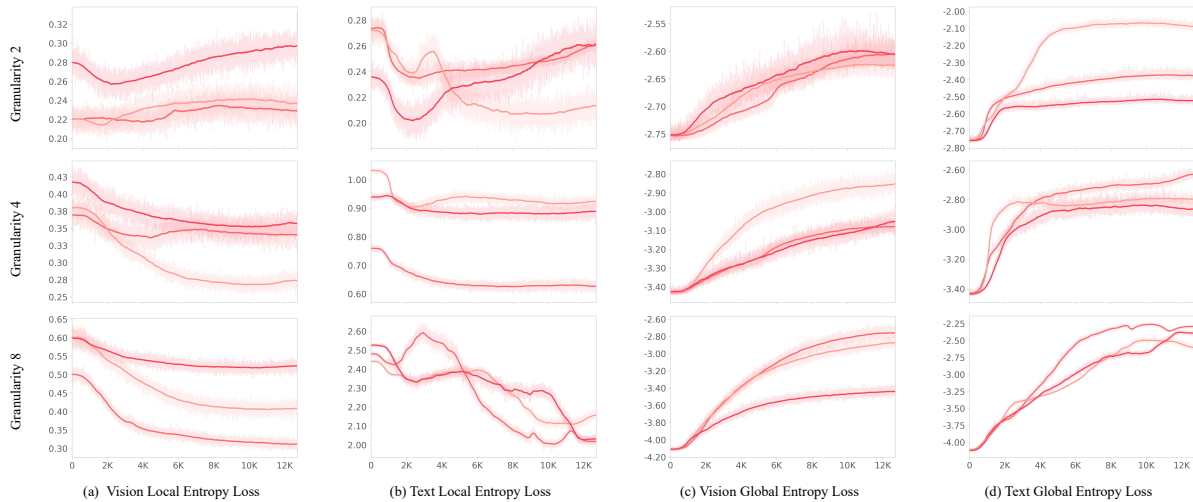


Figure 7. Entropy-based monitoring of router behavior on MOSEI during the Selection stage. We visualize the dynamics of local and global entropy losses for both vision and text modalities across different granularity levels ($\chi = 2, 4, 8$).

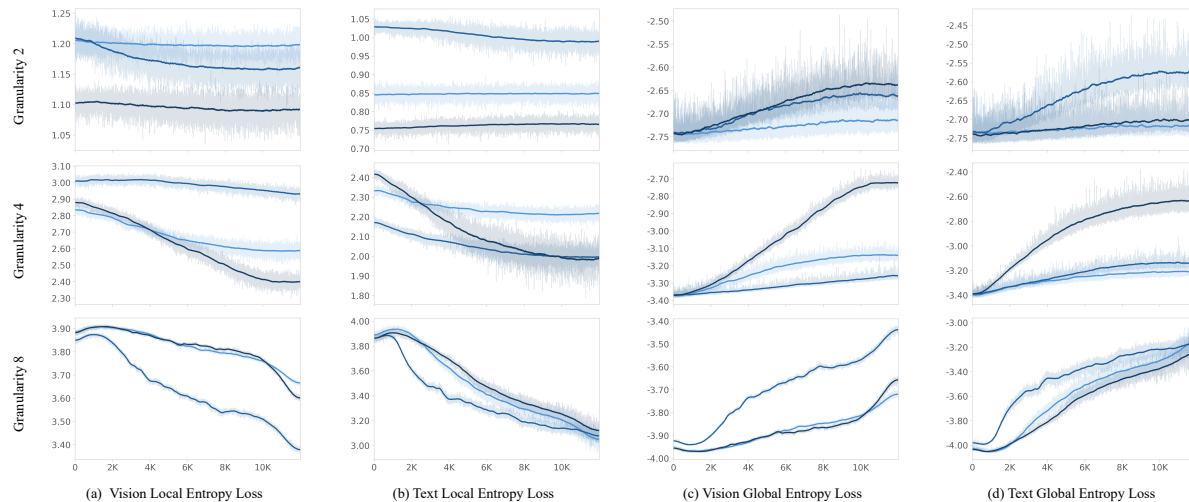


Figure 8. Entropy-based monitoring of router behavior on MOSI during the Selection stage. We visualize the dynamics of local and global entropy losses for both vision and text modalities across different granularity levels ($\chi = 2, 4, 8$).

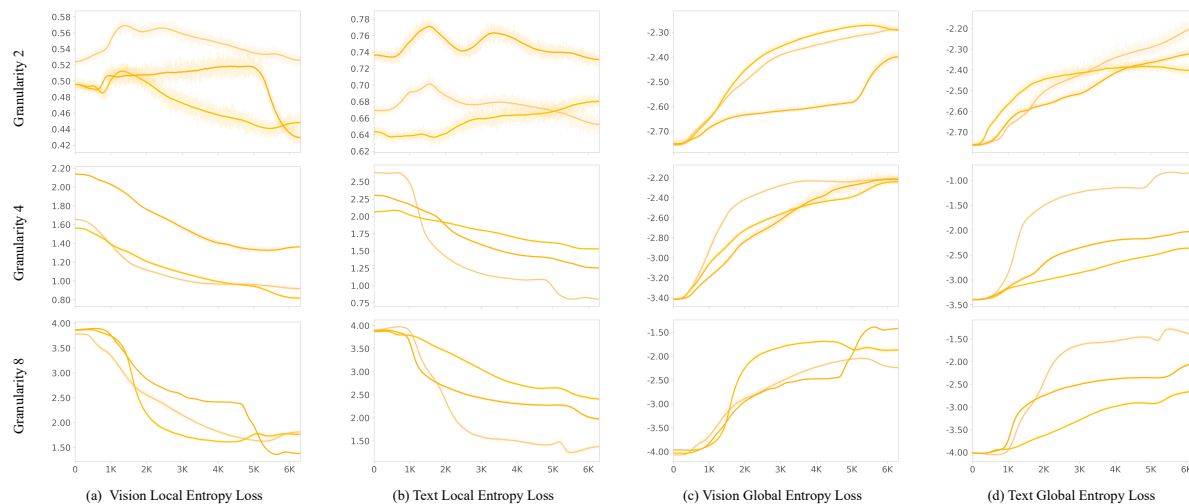


Figure 9. Entropy-based monitoring of router behavior on UR-FUNNY during the Selection stage. We visualize the dynamics of local and global entropy losses for both vision and text modalities across different granularity levels ($\chi = 2, 4, 8$).

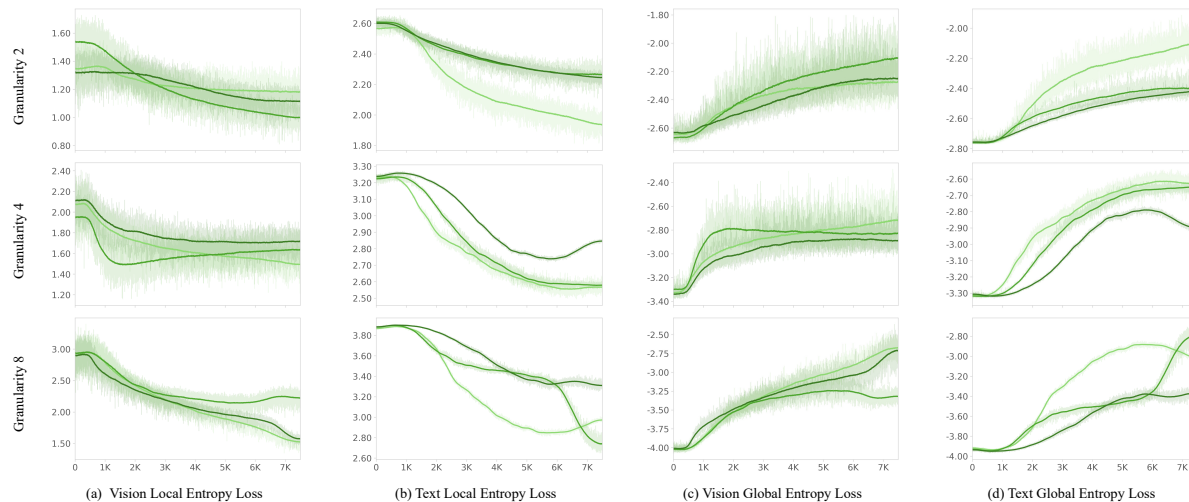


Figure 10. Entropy-based monitoring of router behavior on MUSTARD during the Selection stage. We visualize the dynamics of local and global entropy losses for both vision and text modalities across different granularity levels ($\chi = 2, 4, 8$).